Master of Science

Polymerization of Hollow Core-Shell Particles with Graphene Nanoplatelets and Their Electrochemical Performance

The Graduate School of University of Ulsan

School of Chemical Engineering

Jin Yeong Kim

Polymerization of Hollow Core-Shell Particles with Graphene Nanoplatelets and Their Electrochemical Performance

Supervisor: Professor Eun Suok Oh

A Dissertation

Submitted to
the Graduate School of the University of Ulsan
In partial Fulfillment of the Requirements
for the Degree of

Master

by

Jin Yeong Kim

School of Chemical Engineering
University of Ulsan, Korea
February 2020

Polymerization of Hollow Core-Shell Particles with Graphene Nanoplatelets and Their Electrochemical Performance

This certifies that the master's thesis

of Jin Yeong Kim is approved.

Committee Chair Prof. Won Mook Choi

Committee Member Prof. Sung Gu Kang

Committee Member Prof. Eun Suok Oh

School of Chemical Engineering

University of Ulsan, Korea

February 2020

Acknowledgement

During my graduate life, I have a lot of people to be thankful.

I could have done this research thanks to all of my lab members who have taught and helped me to finish this work since I was just a beginner. Especially I'd like to express the best gratitude to professor Eun Suok Oh. If I hadn't met him, my graduate life would have been very different because he developed me by giving many opportunities. He gave a lot of advice and learning opportunities such as English conversation. Above all, he generously supported my research life. Finally, I want to express my gratitude to all of my friends and dear people. They've always been around me and they've given energy to me. Because of their help, I was able to overcome many difficulties.

With the help of many people, I could grow even more. Thank you.

Abstract in Korean

리튬 이차전지는 휴대용 전자기기에서 전기자동차, 에너지 저장 장치와 같은 대형 배터리로 발전해오고 있으며 그에 따라 전지에 대한 연구는 점점 더 활발히 진행되고 있다. 그러나 연구의 대부분은 활물질, 전해질, 분리막에 집중되어 왔으며 바인더의 연구는 비교적 많이 이루어지지 않았다. 전극 내 바인더와 같은 접착물질은 활물질들간 그리고 활물질과 집전체 사이의 응집력을 제공함으로써 높은 기계적 강도와 전기화학적 안정성을 가지게 한다. 그러므로 전지의 안정성 및 성능 향상을 위해서 바인더는 없어서는 안 될 요소이며 그 연구는 필수적이다.

최근 hollow core-shell (HCS) 등의 고분자 입자들이 hollow 구조의 특성상 가질 수 있는 뛰어난 물리적, 화학적 특성과 높은 안정성을 바탕으로 여러 분야에서 연구개발이 진행되고 있으며 전지 분야에서 역시 차세대 바인더로 주목받고 있다.

본 연구에서는 hollow 구조의 전도성 고분자 복합체 바인더를 중합하고 이를 리튬 이차전지 음극 및 전기이중층 커패시터에 적용하여 상용화된 수분산 SBR 타입의 바인더와 비교분석을 진행하였다. 먼저, graphene nanoplatelets (GnP)을 sonication 시켜 물에 분산시킨 후, 그에 MMA-BA-MAA 공중합체 core 와 St-BA-AN 공중합체 shell 을 유화중합하여 core-shell (CS)을 제조하였고, hollow 구조를 얻기 위해 core 를 제거하는 알칼리제이션 과정을 거침으로써 최종적으로 GnP/HCS 복합체 바인더를 제조하였다. 그 후, GnP/HCS 복합체 바인더의 성능을 확인하고자 리튬 이차전지의 lithium titanium oxide (LTO)와 silicon/graphite (Si/C) 음극 및 전기이중층 커패시터의 활성탄 전극에 각각 적용하였고, 사이클 수명, 율속 특성, 임피던스 등의 전기화학적 분석과 FT-IR, Raman, adhesion test, electrolyte uptake 등의 물리적 분석을 실시함으로써 CS, HCS 그리고 상용화된 SBR 타입의 바인더 (400B)와 비교 분석하였다.

Abstract in English

Lithium ion batteries (LIBs) have evolved from portable electronic devices to larger batteries such as electric vehicles and energy storage system. This indicates that research on batteries, including electrode composite materials, is becoming more active nowadays. However, most of the research has been focused on active material, electrolyte and separator. The study of binder has not been done much. It is already known adhesive elements, such as binder, provide cohesion between active materials and adhesion between active materials and current collector to have the strong mechanical ability and long-term electrochemical stability. Therefore, binder is an integral part of improving battery stability and performance, and the research is essential.

Recently, polymer particles such as hollow core-shell (HCS) are under research and development in various fields, and HCS polymer particles are also seen as attractive binders in the battery field based on the excellent physical and chemical characteristics and the high stability of hollow structure.

In this study, conductive polymer complex binder with hollow structure was polymerized and the synthetic polymer was examined as a new water-treated conductive binder for various anodes of LIBs and electric double-layer capacitors (EDLCs) compared with commercial water-treated SBR type binder. First, the graphene nanoplatelets (GnP) were dispersed by sonication to the water and then MMA-BA-MAA copolymer core and the St-BA-AN copolymer shell were polymerized by in-situ polymerization method with a thermal initiator system to manufacture the core-shell (CS), and finally alkalization was carried out to remove the core for the hollow structure. Then, to check the performance of the GnP/HCS binder, it was applied to lithium titanium oxide (LTO) and silicon/graphite (Si/C) anode of LIBs and activated carbon electrode of EDLCs, respectively. And finally it was compared and analyzed with the CS, HCS and commercialized SBR type binder (400B) by performing electrochemical analysis of cycle performance, rate capability and electrochemical impedance spectroscopy and physical analysis of FT-IR, Raman, adhesion test and electrolyte uptake and so on.

Contents

2. Experimental

Figure list

Figure 24. EIS results of activated carbon electrodes.

Table list

1. Introduction

1.1. Lithium ion batteries (LIBs)

When we use the energy, batteries convert stored chemical energy into electrical energy by electrochemical reactions. In other words, the batteries are energy storage devices. Batteries can be divided into primary batteries and secondary batteries. The biggest difference between them is that the primary batteries such as mercury dry battery can only be used once, and the secondary batteries can be used again through charging.

A type of secondary batteries, lithium ion batteries (LIBs) are composed largely of anode, cathode, electrolyte and separator. And one electrode is made up of active material, conductive material and binder. LIBs produce energy by redox reaction of lithium ions. When LIBs are charged, that is, when they store energy, lithium ions are released from the cathode and passed through the electrolyte and separator finally entered the anode by external force. The discharge process of LIBs is completely the opposite of charge process, meaning energy is generated. Therefore, in order to improve the efficiency of LIBs, it is necessary to use electrode materials that can store large amounts of lithium ions and that can produce rapid reaction with lithium ions. Active materials such as LCO and LFP are usually used for cathode and active materials such as LTO and graphite are usually used for anode. Also silicon has recently been drawing attention due to its potential as anode active material. The separator is an important part of preventing electric shocks by blocking contact between the two electrodes. Polyethylene or polypropylene is usually used as separator. $LiPF_6$ dissolved in a carbonate solvent is usually used as electrolyte. [1, 2]

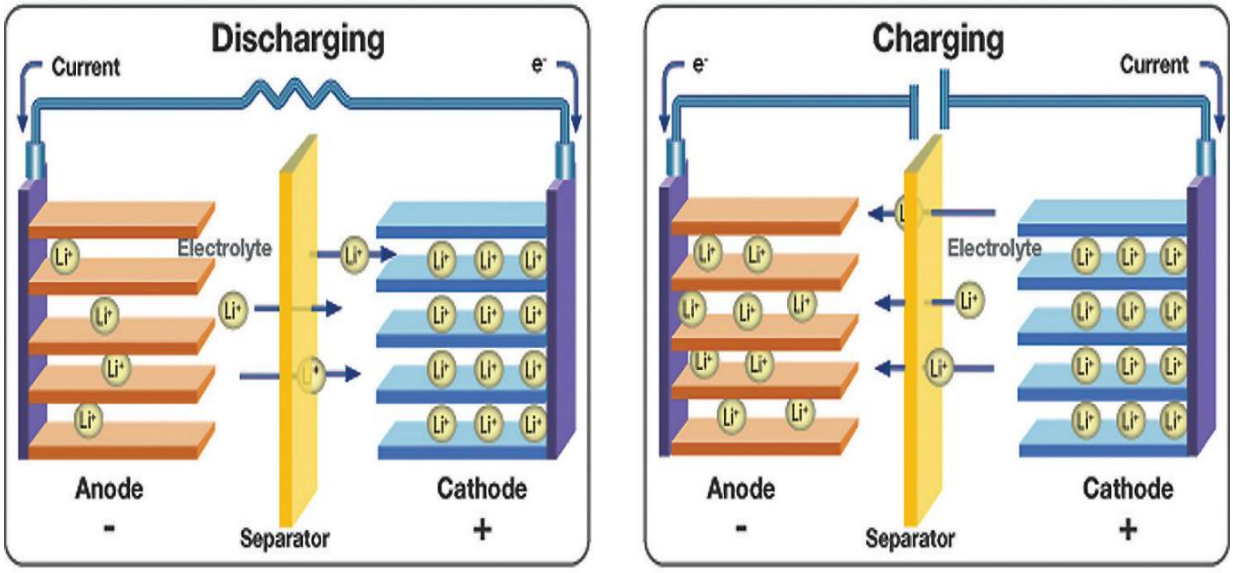

Figure 1. Schematic illustration of charge/discharge process of LIBs.

1.2. Electric double-layer capacitors (EDLCs)

Electric double-layer capacitors (EDLCs) are also a type of energy storage devices by using pseudo-capacitance caused by reversible faradaic redox reaction at the interface between electrode and electrolyte and electrochemical double-layer capacitance caused by charge separation between electrode and electrolyte. EDLCs can retain outstanding capacitance [Farad:F] as well as maintain both conventional electrostatic and electrolytic capacitor's characteristics. And also EDLCs have a higher power density compared to LIBs.

EDLCs are composed of cathode, anode, electrolyte and separator. Cathode and anode materials are usually same so they are called as symmetric EDLCs. The activated carbons are used as active materials for EDLCs because of their tremendous specific surface area, chemical resistance, low thermal expansion, high electrical conductivity and low cost. The electrolyte plays a role of charge carrier as ionic liquid phase. The separator has role of the division for both cathode and anode by using a porous membrane of cellulose system. When EDLCs are charged by the external voltage, electrons are attracted to the positive electrode and electrons are repelled from the negative electrode. Then the conducting plate connected with the positive electrode would be (+) charge and the conducting plate connected with the negative electrode would be (-) charge. Therefore, the voltage difference is formed between the two electrodes. When EDLCs are discharged, electrons start to move to plate having a higher potential. The flow of electrons is continued until there is no electron at the plate. In electrolyte, while EDLCs are charged, cations travel towards the negative electrode and anions accumulate near the positive electrode surface. When charges are released, the reverse process takes place. The mechanism of electric double layer determines that no charge transfer or ions exchange happens across the electrode/electrolyte interface. This means that electrolyte concentration remains constant during charge and discharge processes. As a result, energy is stored in electric double-layer interface. [3-6]

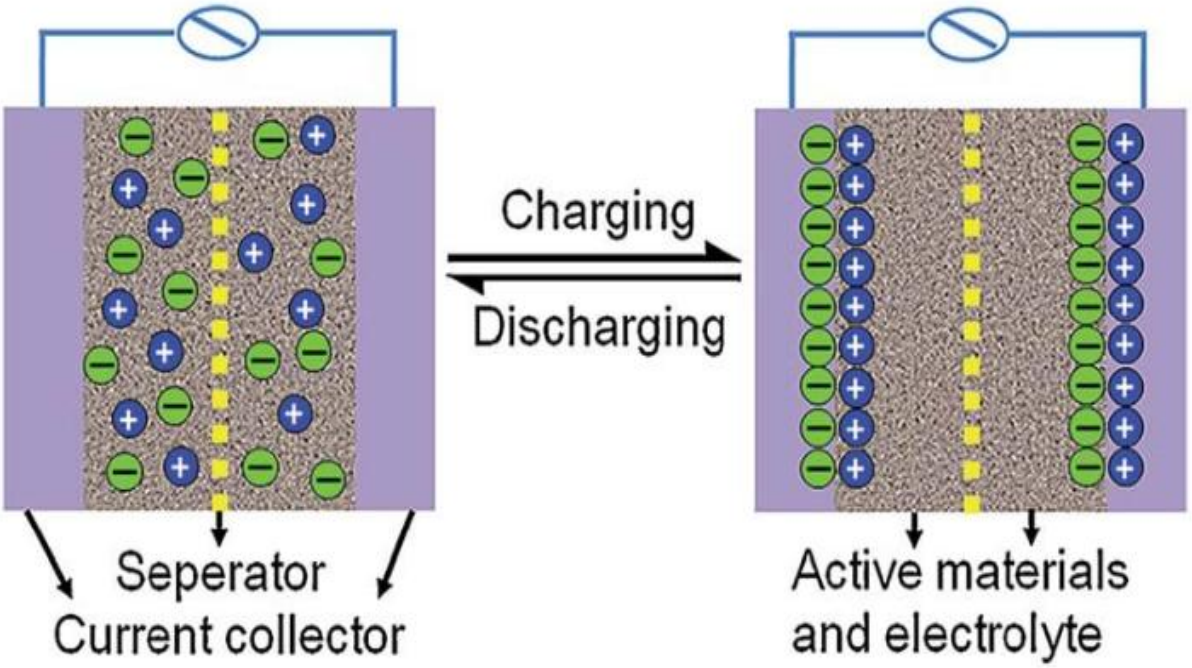

Figure 2. Schematic illustration of charge/discharge process of EDLCs.

1.3. The characteristics of electrode materials

1.3.1. Lithium titanium oxide (LTO)

$Li_4Ti_5O_{12}$ (LTO) has positive aspects for anode of LIBs. First, because LTO has a high and flat lithium insertion voltage, that is, 1.55V vs. Li/Li^+, lithium dendrite growth can be completely blocked then it can be a stable condition. Second, during the charge process, there is very low volume expansion, which is called zero-strain material. Third, it shows exceptional cycling performance with long cycle life. Despite such advantages, however, LTO also has some disadvantages such as lower electronic conductivity and low diffusion coefficient of lithium ions. There have been many studies to overcome these problems, we also want to overcome these problems by manufacturing conductive polymer complex binder with graphene nanoplatelets (GnP) and applying them to LTO anode. [7]

1.3.2. Silicon/graphite (Si/C)

These days, silicon has been drawing attention as an active material of anode due to its high theoretical capacity of 4,200 $mAhg^{-1}$ and studies of silicon are being done in many ways. However, due to the following problems of silicon, it is difficult to commercialize it. First, it has a substantial volume expansion up to 300 % during the charge process. Second, it has low electrical conductivity. Third, the formation of oxide layer happens on silicon surface. Thus, in this study, the graphite, which has a relatively low theoretical capacity of 372 $mAhg^{-1}$ but shows only 7 % volume expansion in the charge process, was mixed with silicon at 3:1 ratio and utilized as an active material of anode. [8, 9]

1.3.3. Activated carbon

The activated carbon has pores of various sizes such as macro, meso and micro, so its surface area is considerably wider than 1000 m^2g^{-1}. Therefore, a large amount of electric charge can be held on its surface. In addition, activated carbon does not produce any reaction on its own within the normal voltage range. Because of these reasons, activated carbon is mainly used in electrodes for capacitor operating at 0.1 V-2.7 V. [10]

1.4. Necessity of binder research

Binder is an essential element despite its small use in electrodes because it significantly affects the stability and high performance of electrodes. Binders such as PVdF, SBR, and CMC have been used primarily in LIBs. In LIBs, binder should have the following properties: First, cohesion between active materials and adhesion between active materials and current collector (i.e. the Al foils, Cu foils) should be ensured. Second, binder itself must be chemically, electrochemically and thermally stable in the electrode/electrolyte interaction over the full range of the battery's operating voltage to perform the essential properties and functions. In general, binder is a media that is electrochemical inactivity.

Nevertheless, polymer binders are expected to absorb electrolyte and have some lithium ions conductivity. Recently, polymer particles such as HCS are under research and development in various fields such as dyes and pharmacology. HCS polymer particles are also seen as attractive binder in the battery field based on their outstanding physical and chemical properties from their hollow structure. They are expected to increase the stability and adhesive strength of electrodes. Electrolyte uptake is also expected to be increased from their hollow structure.

In this study, conductive polymer complex binder, GnP/HCS, was manufactured by in situ-polymerization, that is, HCS polymer particles composed of core (P(MMA-BA-MAA)) and shell (P(St-BA-AN)) with GnP were polymerized. The reason why St, BA and AN were used as shell materials with GnP having an electrical conductivity was their high adhesive strength and flexibility. The synthetic binder was applied in electrodes of LIBs and EDLCs. Finally, it was compared and analyzed with CS, HCS and SBR type binder (400B). [11-16]

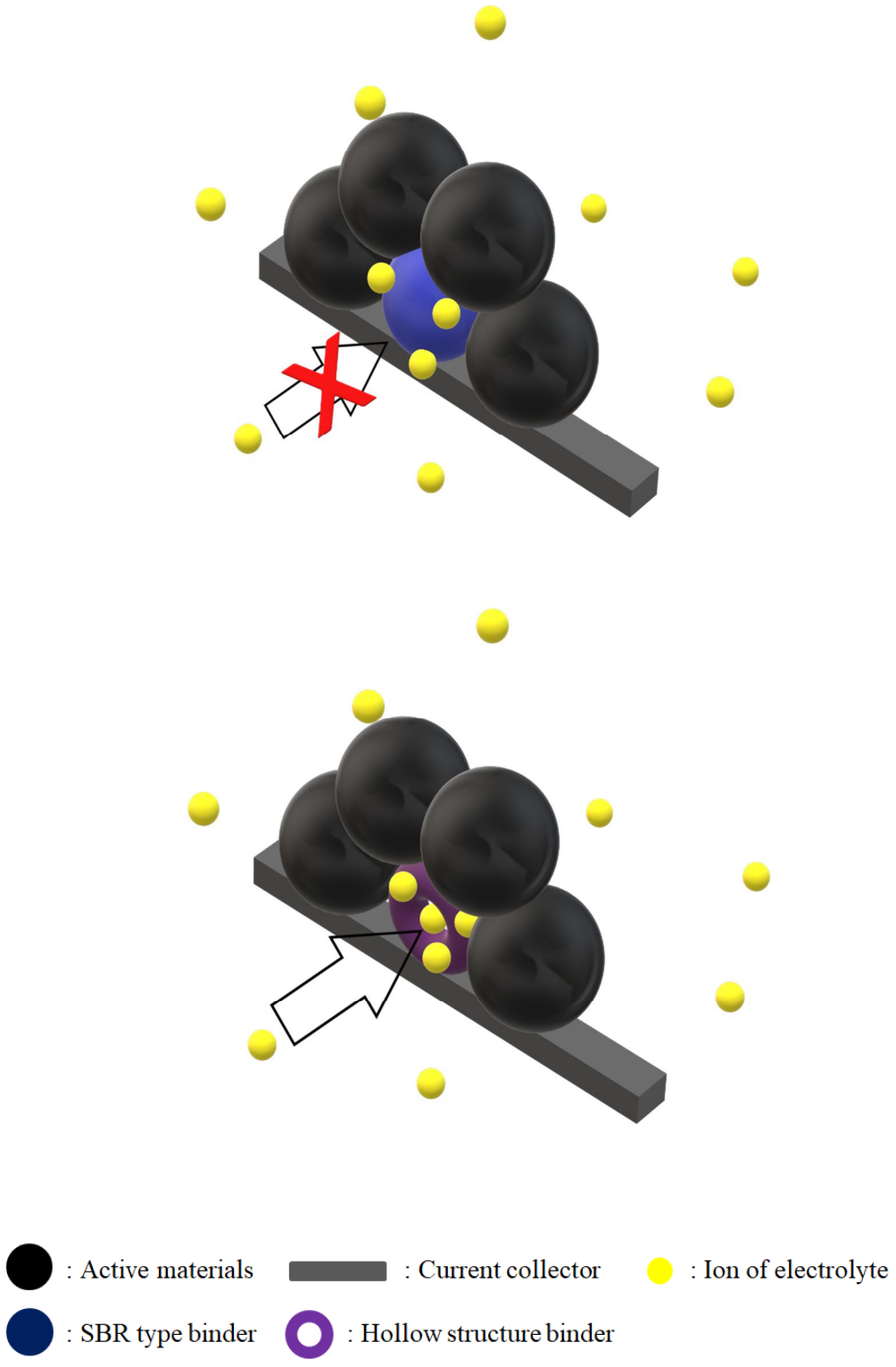

Figure 3. Schematic illustration of the effect of the hollow structure of binder.

2. Experimental

2.1. Fabrication of graphene nanoplatelets (GnP)/hollow core-shell (HCS) binder

2.1.1. Materials

Graphene nanoplatelets (GnP, DEOKYANG) was used after dispersing it in distilled water in advance. Methyl methacrylate (MMA, Sigma Aldrich), methacrylic acid (MAA, Sigma Aldrich), butyl acrylate (BA, SAMCHUN), styrene (St, SAMCHUN) and acrylonitrile (AN, JUNSEI) were used as core-shell monomers. Divinylbenzene (DVB, Sigma Aldrich) was used as crosslinking agent. Ammonium persulfate (APS, Sigma Aldrich) was used as initiator. Sodium dodecylbenzene sulfonate (SDBS, Sigma Aldrich) was used as surfactant. 15 wt% of sodium hydroxide solution was used for alkalization treatment after making core-shell.

2.1.2. Polymerization of GnP/HCS binder

The emulsion polymerization was carried out using a four-neck double jacket flask reactor with a mechanical stirrer, reflux condenser, feeding pump and nitrogen gas purging system. The amount of GnP, monomers and all of other additives used in GnP/CS latex is shown in Table 1. Before starting CS polymerization, as much as 0.5 wt% of CS monomer, GnP was dispersed in distilled water using sonication. The sonication was conducted for 4 hours with the addition of ice every hour. Then three stages of GnP/CS polymerization began. First, in seed stage, seed emulsion was polymerized by continuously feeding pre-mixed monomers and all of other additives to the GnP solution reactor for 2 hours at set temperature. Second, in core stage, core emulsion was also polymerized in the same way as seed stage, adding monomers and other additives to some seed emulsion. Finally, in shell stage, monomers with crosslinking agent solution and other additives with distilled water were separately fed into the reactor that contained some core emulsion for 3 hours. Nitrogen purge was carried out at all of stages and the stirring speed was maintained at 200 rpm. [12-14]

2.1.3. Alkalization treatment

Alkalization treatment was performed to remove the MMA-BA-MAA copolymer of core part as shown in Table 1. The GnP/CS emulsion mixed with 15 wt% NaOH solution was put into a 100 ml vial and stirred by heating-magnetic stirrer at a speed of 1000 rpm at 90 . The MMA-BA-MAA copolymer was ionized by neutralization reaction and the ionized carboxyl salt became MMA-BA-R-COO^-. At this time, the viscosity was increased significantly as ionized core polymer was dissolved in water. Therefore, surfactant and water additions were needed. [12-14]

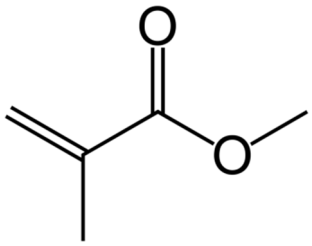

Methyl methacrylate(MMA)

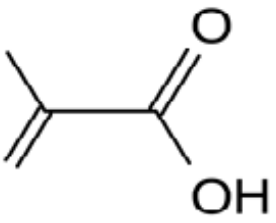

Methacrylic acid(MAA)

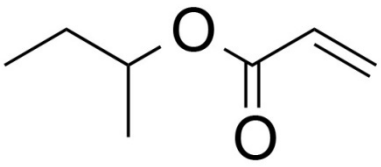

Butyl acrylate(BA)

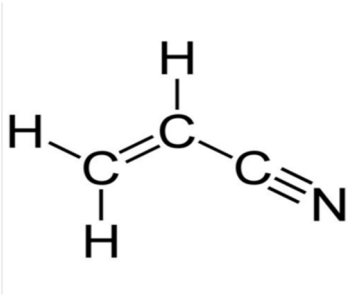

Acrylonitrile(AN)

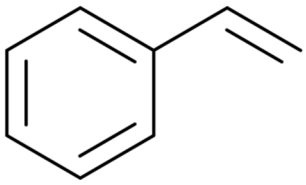

Styrene(St)

Divinyl benzene(DVB)

Figure 4. Chemical structure of materials.

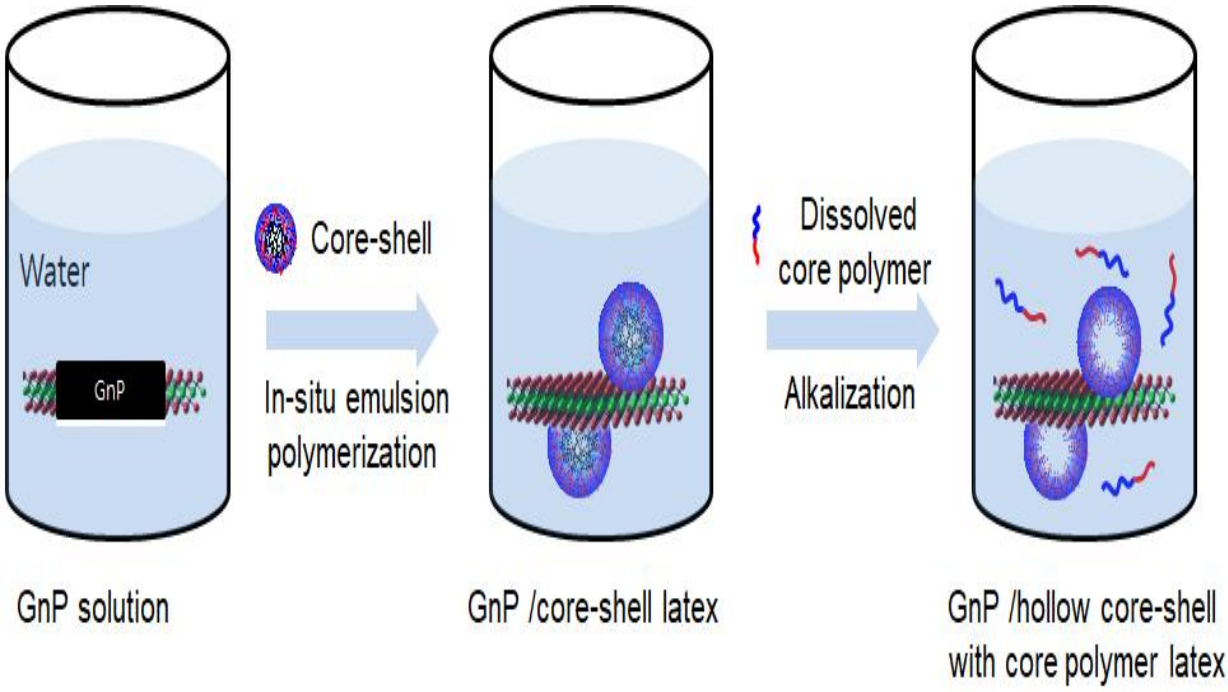

Figure 5. Schematic illustration of polymerization of GnP/HCS binder.

Components	Seed latex (g)	Core latex (g)	Shell latex (g)	Alkalization treatment (g)
GnP	0.57	-	-	-
MMA	5.5	23	-	-
MAA	0.56	10	-	-
BA	6.5	-	40	-
St	-	-	40	-
AN	-	-	20	-
DVB	-	-	1	-
APS	1.0	0.562	0.8	-
SDBS	0.06	0.099	0.2	0.1
Seed latex	-	50	-	-
Core latex	-	-	130	-
Shell latex	-	-	-	30
Distilled water	500.0	250	55	20
15wt% NaOH sol.	-	-	-	5
Temperature/	80	80	75	90

Table 1. Recipe for seed, core, shell latex and alkalization treatment with GnP.

2.2. Preparation of electrodes

2.2.1. LTO electrodes (LIBs)

The preparation process of LTO (POSCO ESM Co., Ltd., Korea) electrodes was conducted by mixing slurry, coating and drying. Slurry of the LTO electrodes was composed of 80 wt% of active materials, 10 wt% of conductive materials, that is, carbon black (super P), 2 wt% of carboxymethyl cellulose (CMC, Sigma aldrich) to control the viscosity and 8 wt% of binder. The slurry was mixed by planetary ball mill mixer (PULVERISETTE 7, FRITSCH). First, all materials except binder were mixed under conditions of 380 rpm, 8 minutes rotation and 5 times. Then binder and small amount of distilled water were added and finally mixed under conditions of 380 rpm, 5 minutes rotation and twice. The mixed slurry was coated with a coating speed of 10 mms^{-1} on Al foil of 20 μm and dried for 30 minutes at convection oven of 60 . Before electrodes were used to make LIB cells, the electrodes were slit in width of 2 cm, then pressed by roll press machine and eventually dried for one day at a vacuum oven of 70 .

2.2.2. Si/C electrodes (LIBs)

Si/C electrodes were also prepared in the same order as LTO electrodes. Slurry of Si/C electrodes was composed of 76 wt% of silicon and graphite (1:3 ratio) as active materials and 9 wt% of the conductive materials (super P), 5 wt% of CMC (CMC, Sigma aldrich) and 10 wt% of binder. The slurry was mixed by planetary ball mill mixer under the same conditions with LTO. The mixed slurry was coated with a coating speed of 10 mms^{-1} on Cu foil of 18.4 μm and dried for 30 minutes at convection oven of 60 . Before electrodes were used to make LIB cells, the electrodes were slit in width of 2 cm, then pressed by roll press machine and eventually dried for one day at a vacuum oven of 70 .

2.2.3. Activated carbon electrodes (EDLCs)

Activated carbon electrodes for EDLCs were also prepared in the same order as above electrodes. Slurry of activated carbon electrodes was composed of 90 wt% of activated carbon (YP-50, Kuraray) as active materials and 4 wt% of the conductive materials (super P), 1.5 wt% of CMC (WS-C, Dai-lchi Kogyo Seiyaku Co.) and 4.5 wt% of binder. The slurry was mixed by planetary centrifugal mixer (ARE-310, THINKY). The mixed slurry was coated with a coating speed of 10 mms^{-1} on etched Al foil and dried for 30 minutes at convection oven of 60 . Before electrodes were used to make EDLC cells, the electrodes were slit in width of 2 cm, then pressed by roll press machine and eventually dried for one day at a vacuum oven of 70 .

Electrodes composition

	Active material (%)	Conductive material (%)	Binder (%)
LTO	80	10	10
Si/graphite	76	9	15
YP-50	90	4	6

Table 2. Weight percent ratio of electrode slurry.

Planetary ball mill

Planetary centrifugal mixer

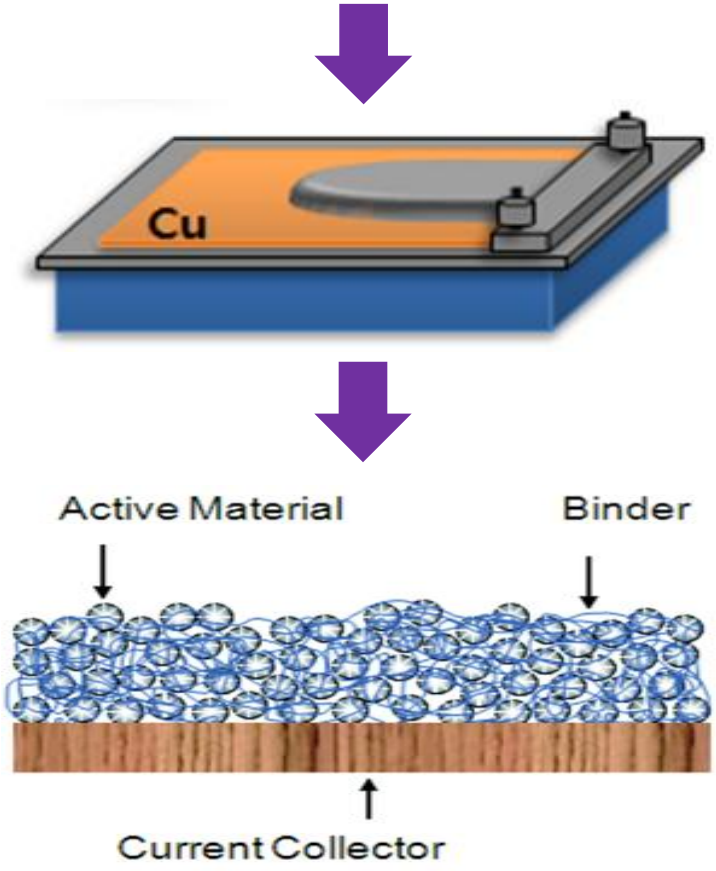

Figure 6. Manufacturing process of the electrodes of LIBs and EDLCs.

2.3. Fabrication of cells

2.3.1. CR 2032 coin cells

CR 2032 coin cell was made up of case, gasket, spacer disk, spring and cap. The coin cells were always made inside argon-filled glove box. The order in which coin cells were made was as follows. First, working electrode, i.e. LTO, Si/C, and activated carbon electrodes, was placed in the case. Second, the separator was placed on the electrode. Third, electrolyte was injected. At this time, in case of LTO, 1M $LiPF_6$ in EC:EMC:DMC=1:1:1 v/v% from Soulbrain, in case of Si/C, 1.15mM $LiPF_6$ in EC:DEC:DMC=3:5:2 v/v% with additives (5 wt% FEC, 2wt% VC and 0.4 wt% $LiBF_4$), in case of activated carbon, 1M tetra-ethylammonium-tetra-fluoroborate ($TEABF_4$) in acetonitrile were used as electrolyte. Fourth, the gasket was placed. Fifth, the counter electrode is located. At this time, lithium metal chip was used for LIBs and the same electrode as working electrode was placed for EDLCs so that both electrodes could be faced each other. Finally, spacer disk and spring were put and the cap was assembled.

2.3.2. HS-3E flat cells

HS-3E flat cell (Welcos), that is, three electrodes system, was used for only cyclic voltammetry (CV) of binder films. Three electrodes of HS-3E flat cell consisted of working electrode of binder film, counter electrode of lithium metal chip and reference electrode of lithium metal wire. Cell assembly was as follows. First, working electrode was placed in the lower body. Second, electrolyte was injected. Third, separator was put. Fourth, insulating guide was placed. At this time, the guide was first assembled with a thinly sliced reference electrode and then placed. Fifth, electrolyte was injected. Sixth, counter electrode was placed. Seventh, metal plate and spring were placed. Finally, reference lead was connected with the reference electrode and upper body then finally assembled.

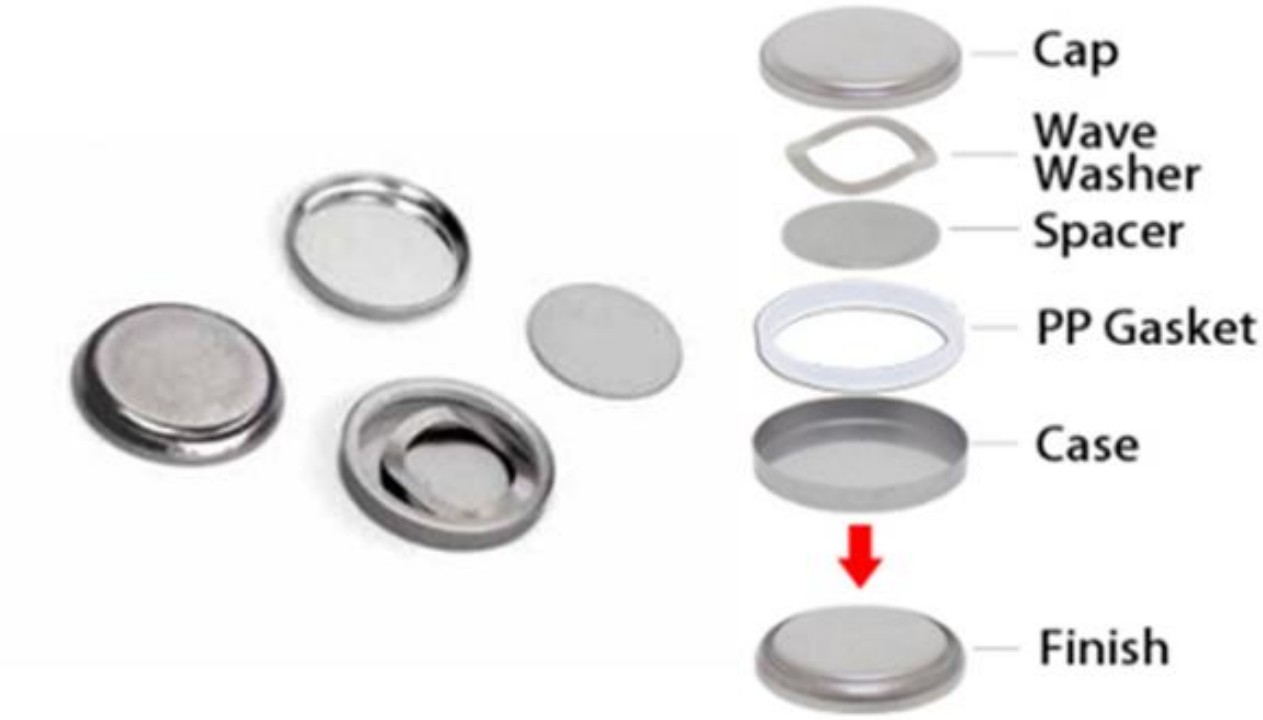

Figure 7. CR 2032 coin cell assembly.

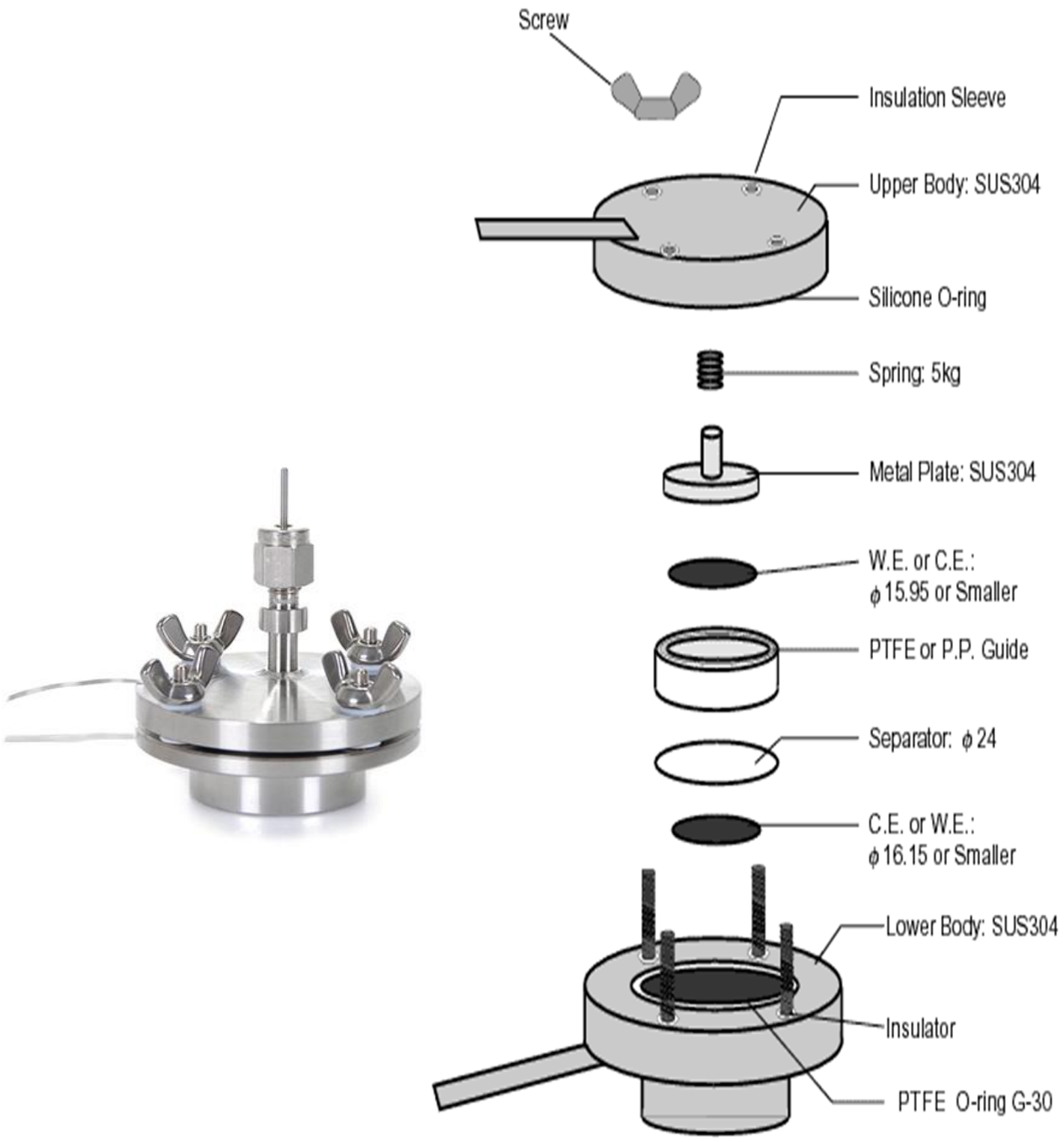

Figure 8. HS-3E flat cell assembly.

2.4. Physical characteristics

2.4.1. Field emission – scanning electron microscopy (FE-SEM)

The morphology of CS, HCS, GnP/CS and GnP/HCS particles was observed by FE-SEM (JSM-6500, JEOL). Dried binder solutions were used.

2.4.2. High resolution – transmission electron microscopy (HR-TEM)

The morphology of CS, HCS, GnP/CS and GnP/HCS particles was observed by HR-TEM (H-8100, Hitachi). Diluted binder solutions were dropped on the copper grid and dried. Dried binder films should be transparent enough for light to pass through the samples.

2.4.3. Raman spectroscopy

Raman spectroscopy (DXR Raman Microscope, Thermo Fisher SCIENTIFIC) was measured to determine the structural fingerprints of binders, i.e. the presence of GnP and hollow structure. Raman spectroscopy was analyzed from 3500 to 500 cm^{-1}.

2.4.4. Fourier transform infrared spectroscopy (FT-IR)

An infrared spectrum represents fingerprints of samples with absorption peaks which correspond to frequencies of vibrations between the bonds of the atoms making up the material. Because each different material has a unique combination of atoms, no two compounds produce the exact same infrared spectrum. Therefore, infrared spectroscopy can result in positive identification of every different kind of material. Alkalization process was analyzed by fourier transform infrared (FT-IR, Nicolet IR 200, Thermo Scientific) spectra from 4000 to 500 cm^{-1} for searching ionized carboxyl salt. The FT-IR was conducted by using potassium bromide pellets.

2.4.5. Zeta potential

Zeta potential (Zetasizer Nano ZS, Malvern Panalytical) is defined as the potential difference between dispersion medium and stationary layer of fluid attached to the particle. Zeta potential was performed using disposable folded capillary cells (DTS1070). This allowed the measurement of the zeta potential and the ionic conductivity. The zeta potential value read the absolute value, and the larger absolute value, the more stable.

2.4.6. Electronic conductivity

EIS (VSP, BioLogic Science Instruments) was performed to measure electronic conductivity of binders. Binder films were coated on etched Al foil and cut to a diameter of 16mm. Coin cells were manufactured with only binder films without electrolyte and lithium chip. The measurements were taken from 1000 khz to 100 hz.

2.4.7. Differential scanning calorimetry (DSC)

DSC (Q20, TA Instruments) was performed to identify the glass transfer temperature (Tg) of binders in nitrogen atmosphere at the heating/cooling speed of 10°Cmin^{-1}. The measurement range was from -30 °C to 200 °C. The binders were placed on the aluminium pans (Tzero Hermetic aluminium pan) and sealed.

2.4.8. Dispersion stability

Dispersion stability of binder solutions was measured by Turbiscan (Ageing characterization :Turbiscan LAB, Formulaction). For 24 hours, the machine injected light to the solution changing height. This machine could measure backscattering, sedimentation, clarification and aggregation etc.

2.4.9. Adhesive strength

Mechanical adhesive strength of coated slurry on the current collector was measured by 180° peel test using a texture analyzer (TA-PLUS, Lloyd Instrument Ltd.). Adhesion is a very important property to withstand deformation caused by volume expansion caused by charging and discharging. Sample preparation was as follows. First, the electrodes were prepared by cutting them to have a width of 2cm. And then, one side of the double sided tape was attached to the metal plate and the other side to the electrodes. The electrodes were pressed twice by rolling machine for uniform pressure. The measurements were made when the upper part of the equipment pulled the electrodes attached to the metal plate and the adhesion was recorded.

2.4.10. Electrolyte uptake

Binders were prepared in a diameter of 14mm and put into vials containing 20 ml of electrolyte (DMC:EMC = 1:1) for 1 h, 6 h, 14 h and 24 h, respectively. The binders were compared in weight before and after being immersed in the electrolyte.

2.5. Electrochemical characteristics

2.5.1. Cyclic voltammetry (CV)

CV (VSP, BioLogic Science Instruments) of binder films was measured using a HS-3E flat cell. The reason for using the three electrodes cell was to reduce the IR drop. IR drop is potential drop caused by solution resistance. In CV, IR drop primarily causes following problems : a shift in peak potential, decrease in the magnitude of current, increase in peak separation. CV was measured at 0.2 mVs^{-1} from 0 V to 3 V. Diffusion coefficient of ions in the cell was calculated by Randle-Sevcik equation.

2.5.2. Galvanostatic charge/discharge test

The electrochemical properties were confirmed by cycle performance and rate capability test. The binders were applied to LTO, Si/C and activated carbon electrodes. In the test of LTO anode of LIBs for the cycle performance, cells were cycled at the rate of 0.1 C for the first 2 cycles and at the rate of 1 C for the subsequent 100 cycles in a range of 1 V - 2.6 V. For the test of rate capability, they were cycled at the rate of 0.1 C, 0.2 C, 0.5 C, 1 C, 2 C, 5 C, 10 C for 8 cycles at each current, finally 0.1 C again for 8 cycles. In addition, the rate capability test of LTO anode without conductive material was performed. They were cycled at the rate of 0.5 C for the first 4 cycles and 1 C, 2 C, 5 C, 10 C for 8 cycles at each current, finally 0.5 C again for 4 cycles.

In the test of Si/C anode of LIBs for the cycle performance, cells were cycled at the rate of 0.1 C for the first 2 cycles and at the rate of 0.5 C for the subsequent 100 cycles in a range of 0.005 V - 2.0 V. For the test of rate capability, they were cycled at the rate of 0.1 C, 0.2 C, 0.5 C, 1 C, 2 C, 5 C, 10 C for 10 cycles at each current, finally 0.1 C again for 10 cycles.

In the test of activated carbon electrode of EDLCs for the cycle performance, capacities were measured first at the rate of 10 mAcm^{-2} from 0.1 V to 2.7 V at which constant voltage mode was done for the first 5 cycles. From the result, 10 mAF^{-1} current was calculated and applied from 1.35 V to 2.7 V, no constant voltage mode, for 5000 cycles. In the test of rate capability of EDLCs, 0.5, 1, 5, 10, 50 and finally 0.5 mAcm^{-2} of current were applied for 20 cycles at each rate. All of above

tests were conducted by battery cycler (PNE solution Co., Korea).

2.5.3 Electrochemical impedance spectroscopy (EIS)

EIS (VSP, BioLogic Science Instruments) was measured from 0.01 Hz to 100 kHz. For the LTO anode of LIBs, EIS of fresh cells was measured at the OCV and EIS of cells charging/discharging from 1 V to 2.6 V was measured at the operating voltage, 1.55 V. For the Si/C anode of LIBs, EIS of fresh cells was measured at the OCV and EIS of cells charging/discharging from 0.005 V to 1.5 V was measured at the operating voltage, 0.2 V. For the EDLCs, EIS of fresh cells was measured at 1.35 V and EIS of cells charging/discharging from 1.35 V to 2.7 V was measured.

3. Results and discussion

3.1. Physical characteristics

3.1.1. FE-SEM and HR-TEM results

Figure 9 is SEM image of CS, HCS, GnP+CS and GnP+HCS. Before alkalization, CS was seen as a ball-shape, while HCS, after alkalization, was seen as a donut-shape. Before alkalization, CS with GnP was seen as similar with just CS shape. After alkalization, however, HCS with GnP was shown with other particles in addition to HCS. It was thought to have originated from GnP. It was difficult to clearly identify the GnP at (c) and (d).

Figure 10 is TEM image of CS, HCS, GnP+CS and GnP+HCS. During alkalization, hollow shells were built because copolymer cores were dissolved out. At that time, several cracks were shown in the shell due to leakage of ionized polymers with COO^- generated from the neutralization of P(MMA-BA-MAA) and hydroxide anion. There was also the difference in color between the core and shell. The binders with GnP, as shown in (c) and (d), a thin film was shown, which was estimated to be GnP.

3.1.2. Raman spectroscopy and FT-IR results

CS, HCS, GnP+HCS and GnP were measured with Raman spectroscopy. As shown in Figure 11, when compared with CS, in HCS and GnP+HCS, a peak was shown at about 1000 cm^{-1}, confirming that alkalization was done properly. In addition, when compared with HCS, in GnP+HCS, D, G, 2D band peaks were shown such as GnP, confirming that GnP was well dispersed.

The FT-IR of CS, HCS, GnP+CS and GnP+HCS were measured. Alkalization process was analyzed by FT-IR for searching ionized carboxyl salt. From Figure 12, after alkalization, that is HCS and GnP+HCS, a peak of ionized carboxyl salts was identified at 1500cm^{-1}-1600cm^{-1}. It showed that P(MMA-BA-MAA) was decomposed into polymer ion with $–COO^{-1}$.

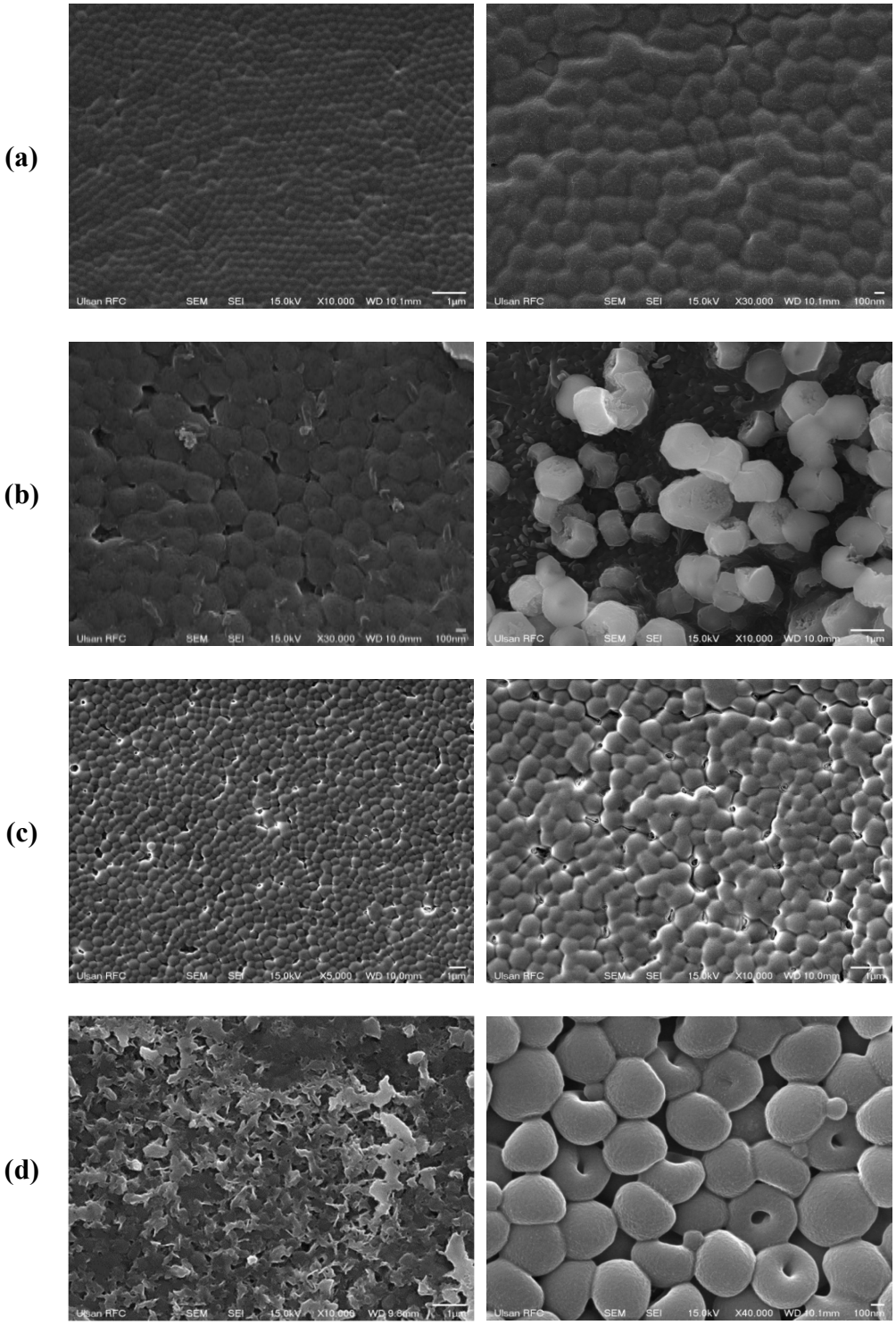

Figure 9. FE-SEM results (a) CS, (b) HCS, (c) GnP+CS, (d) GnP+HCS.

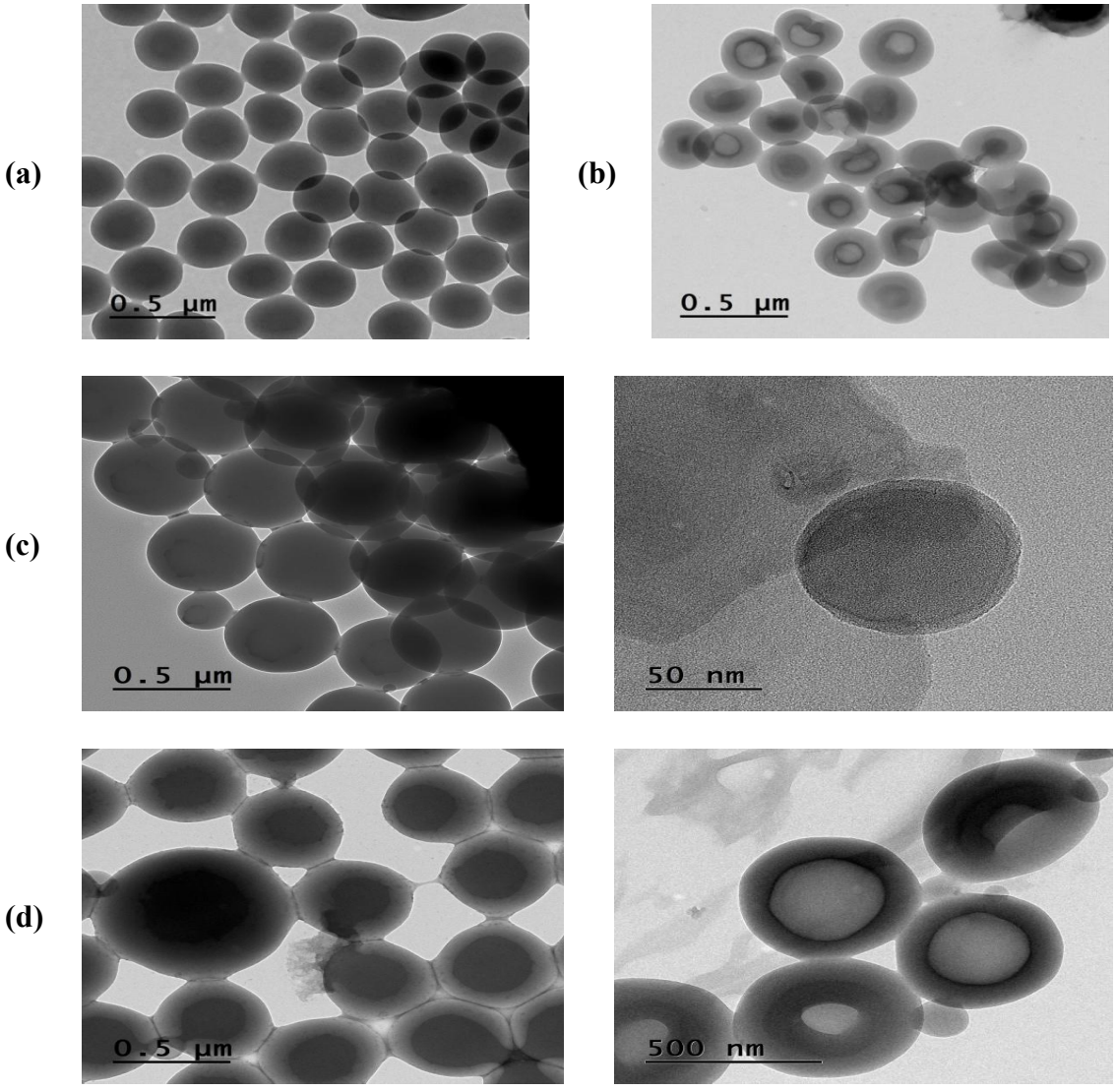

Figure 10. HR-TEM results (a) CS, (b) HCS, (c) GnP+CS, (d) GnP+HCS.

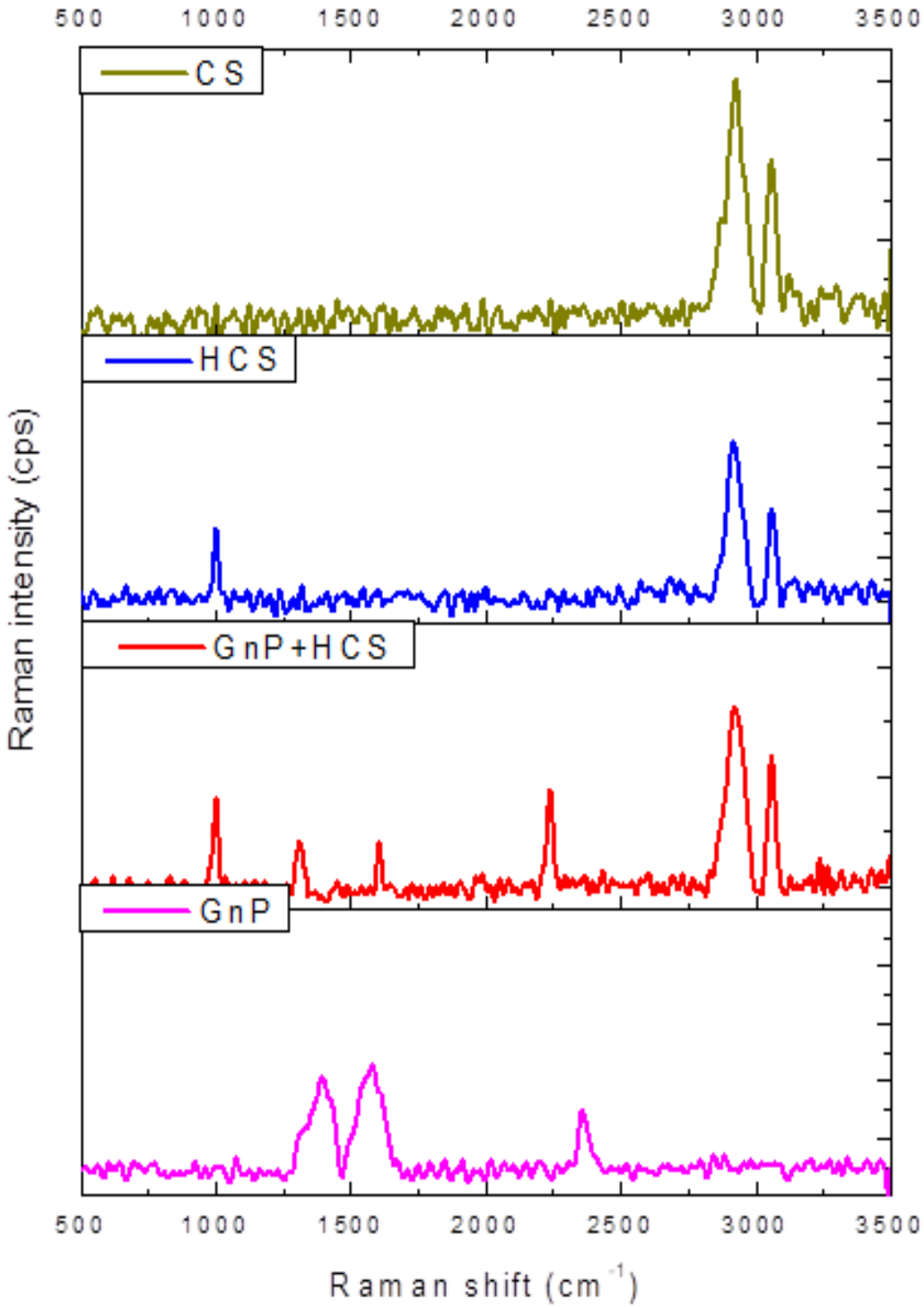

Figure 11. Raman results.

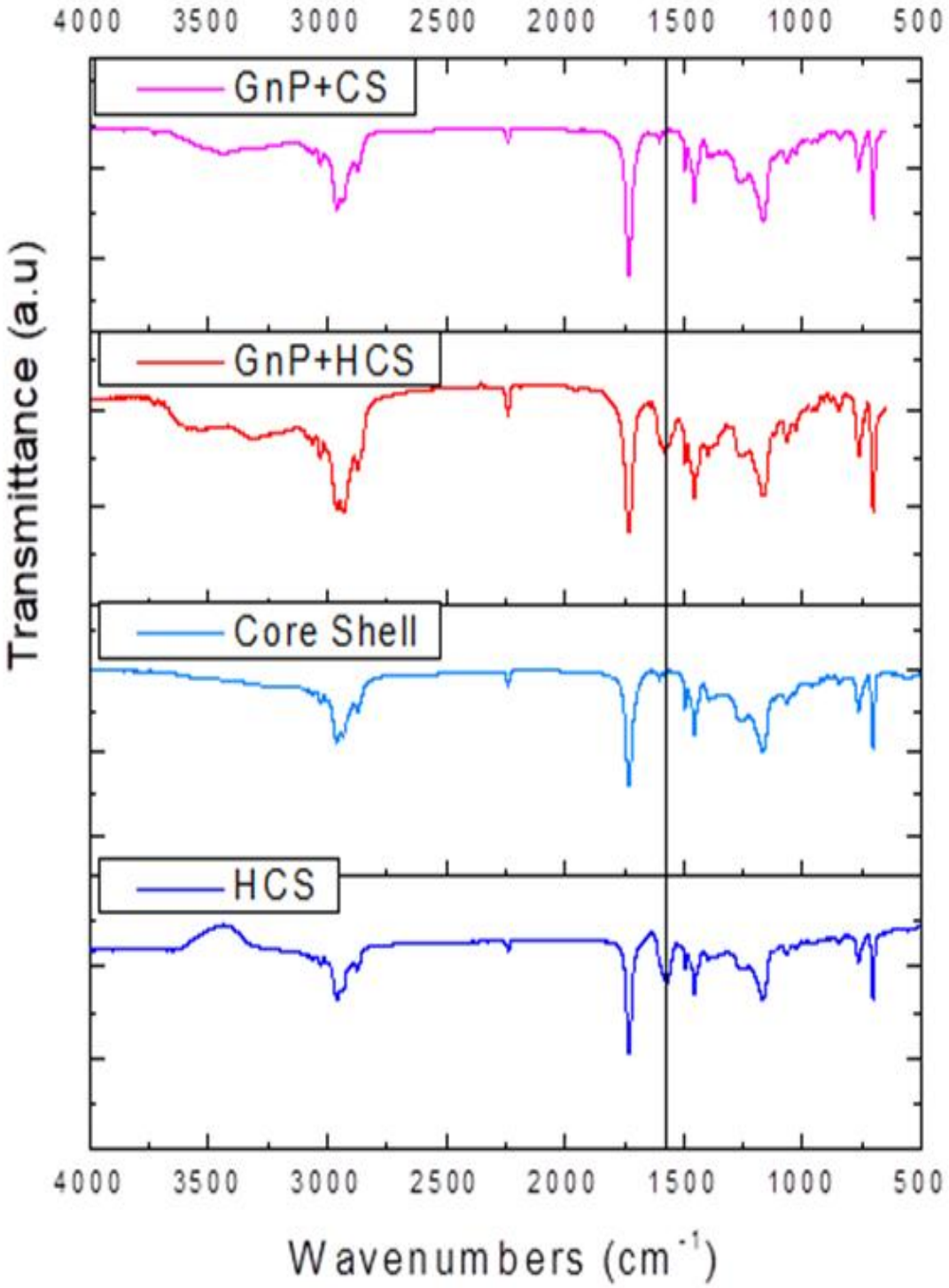

Figure 12. FT-IR results.

3.1.3. Zeta potential results

As shown in Table 3, zeta potential of GnP+HCS was the highest with 8.92. Ionic conductivity of GnP+HCS was also the highest while the ionic conductivity of CS was clearly low. From these results, the following were thought. First, the ions would have moved more easily because of the hollow structure. Second, GnP had influenced conductivity.

3.1.4. Electronic conductivity results

After measurement by EIS, electronic conductivity was calculated by the expression below.

$$\mathrm{R} = \rho\frac{l}{s} \;\rightarrow\; \rho = R\frac{s}{l} \;\rightarrow k = \frac{1}{\rho} = \frac{1}{R \cdot s}$$

It is as follows, ρ:electrical resistivity, l:thickness of the binder film, s:area of the binder film and k:electrical conductivity. As shown in figure 13 and table 4, binder with GnP was found to be more conductive.

3.1.5. DSC results

Since anode is the first heat-response in the battery, it is necessary to consider the glass transition temperature. As shown in figure 14, all showed similar range of glass transition temperatures.

3.1.6. Dispersion stability results

If turbiscan stability index (TSI) is less than 1, the stability of emulsion is excellent. If TSI is less than 3, the stability of emulsion is good. As shown in the figure 15, binders with GnP were more stable than CS, HCS binders. However, the hollow binders couldn't be judged to be more stable than CS binders.

	Zeta potential	Ionic conductivity
CS	**-6.62**	**0.21**
HCS	**-1.04**	**1.22**
GnP+HCS	**-8.92**	**1.46**

Table 3. Zeta potential results.

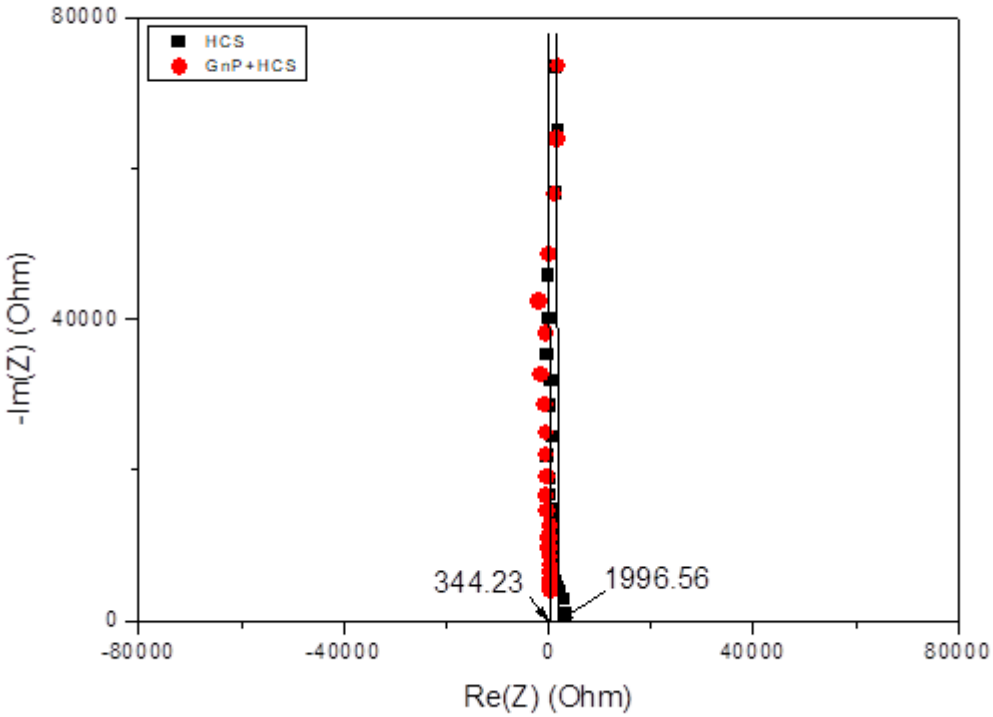

Figure 13. Electronic conductivity results by EIS.

	Electronic conductivity
HCS	**9.04×10^{-7}**
GnP+HCS	**5.82×10^{-6}**

Table 4. Electronic conductivity results by EIS.

(a)

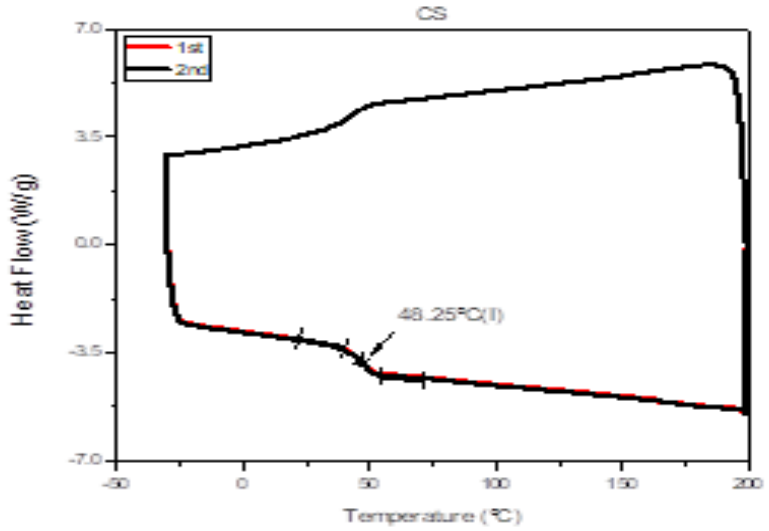

(b)

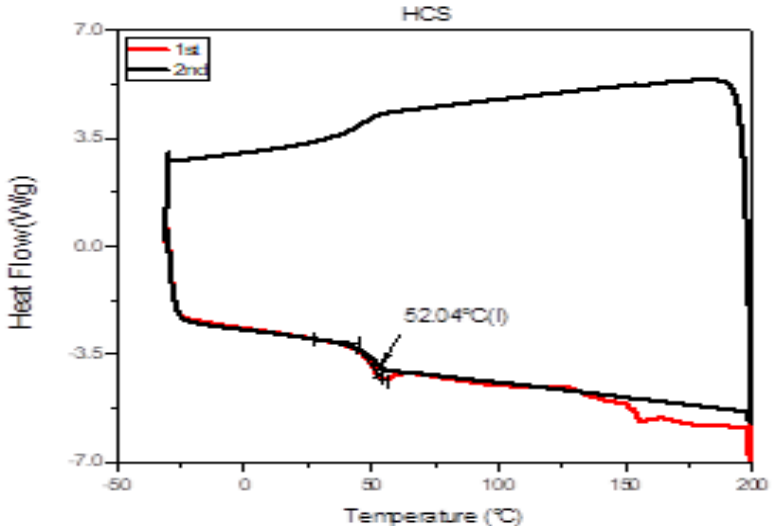

(c)

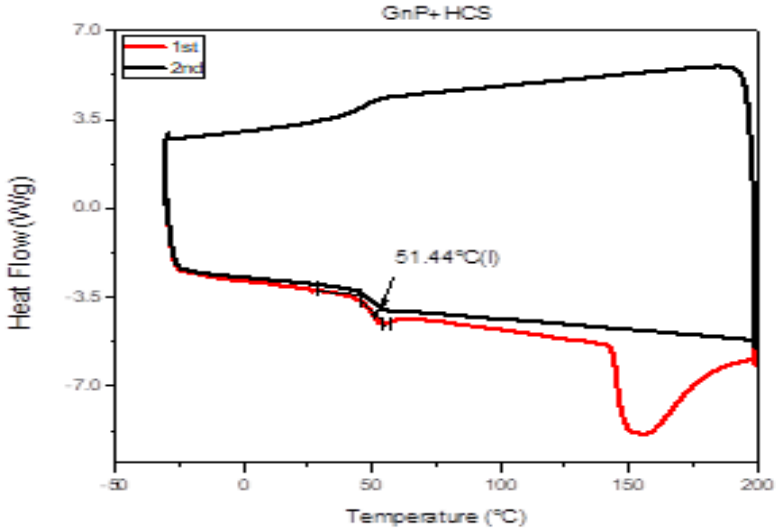

Figure 14. DSC results.

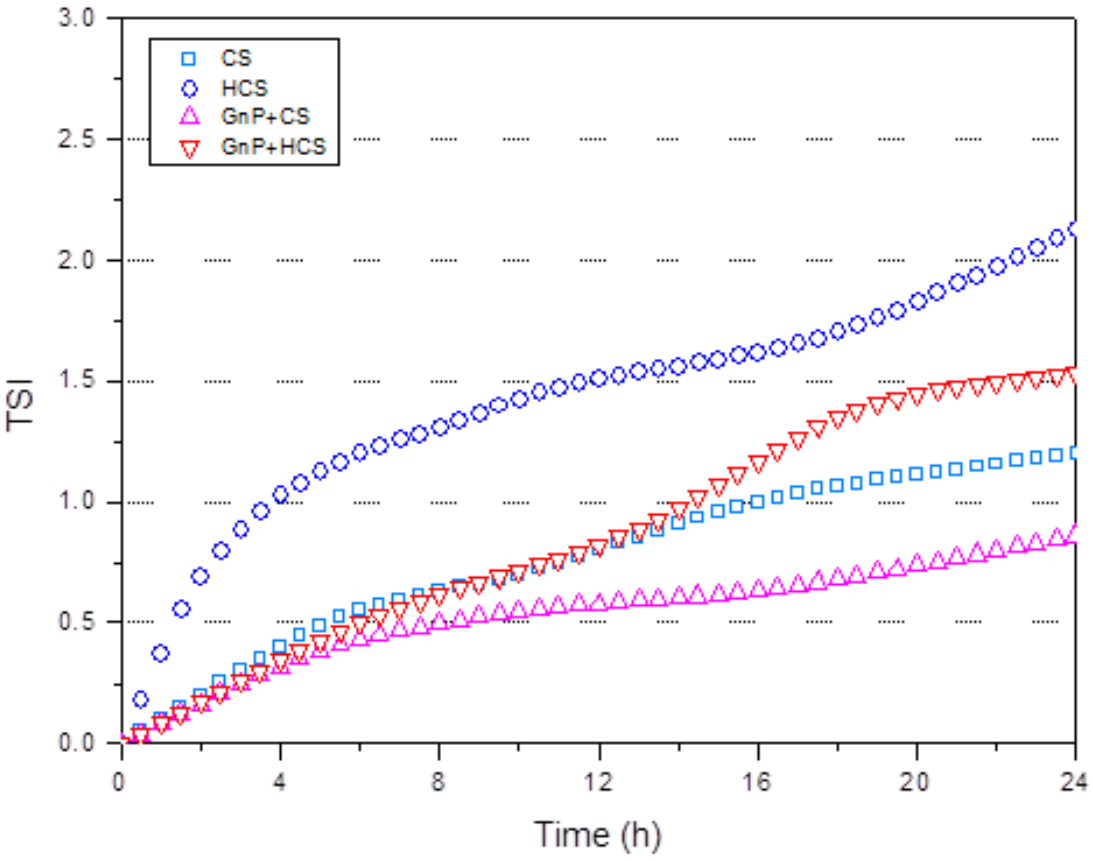

Figure 15. Dispersion stability results.

3.1.7. Adhesive strength and electrolyte uptake results

In adhesive strength test, adhesion of electrodes was absolutely defined except for the effects of all other parameters. The adhesion of LTO, Si/C and activated carbon electrodes to which the binders were applied was measured. For all electrodes, adhesion of 400B, a commercialized binder of SBR type, was the highest. However, regardless of the type of active materials, the adhesion of hollow structure binders was higher than adhesion of CS binder. It was thought that the adhesion of electrodes was increased due to hollow structure.

The electrolyte uptake results showed how much electrolyte binder film could hold inside itself. After being immersed in the electrolyte for one hour, the electrolyte uptake of binders showed similar values except 400B. After being immersed in the electrolyte for six hours, binders of hollow structure showed higher electrolyte uptake than CS binder. After 14 hours, binders of hollow structure still showed higher electrolyte uptake than CS binder and finally after 24 hours, except 400B, also showed same results. Finally, it could be seen that binders of hollow structure, regardless of time, showed higher electrolyte uptake than CS binder. This might be attributed to increased contact area between electrolyte and binder by the hollow structure.

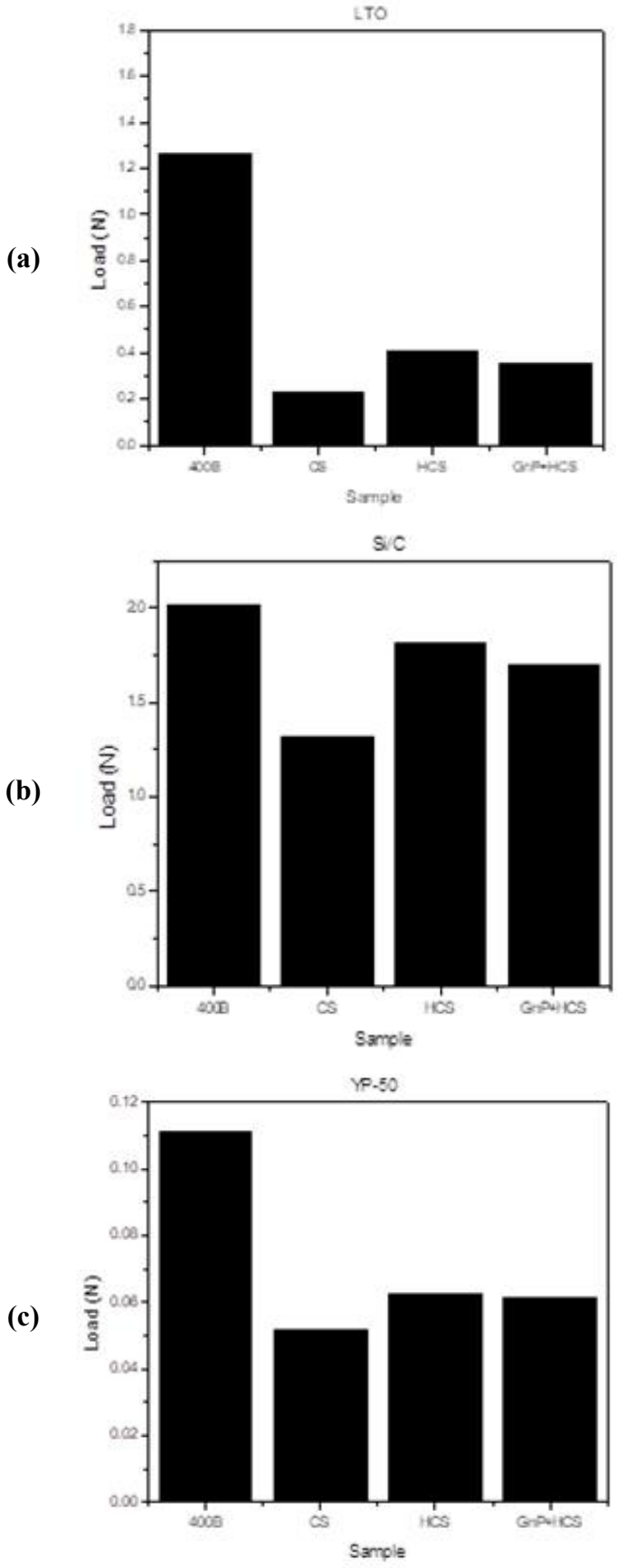

Figure 16. Adhesive strength results.

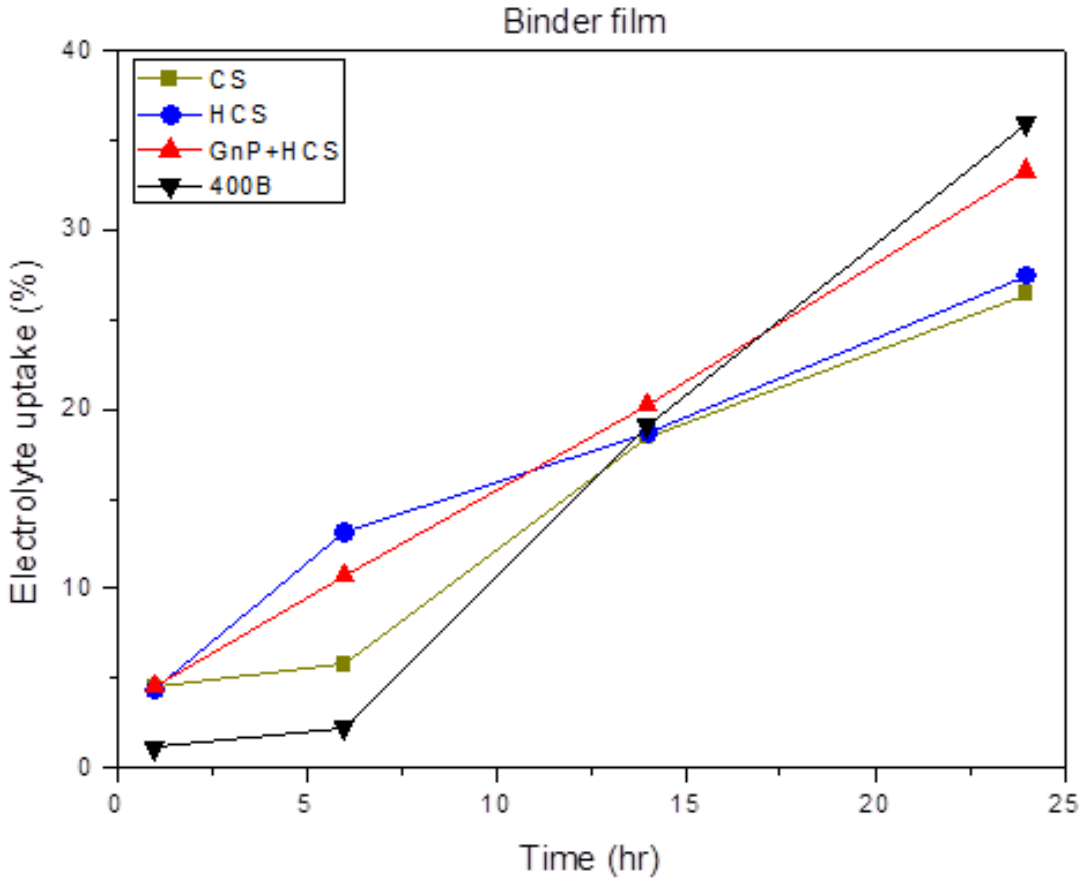

Figure 17. Electrolyte uptake results.

3.2. Electrochemical characteristics

3.2.1. Binder film CV

CV was measured from 0V to 3V to apply as binder to all of electrodes, i.e. LTO, Si/C and activated carbon electrodes. Even though there weren't any active materials and conductive materials, GnP+HCS binder film showed much higher current than HCS binder film. This was thought to be the effect of conductivity of GnP.

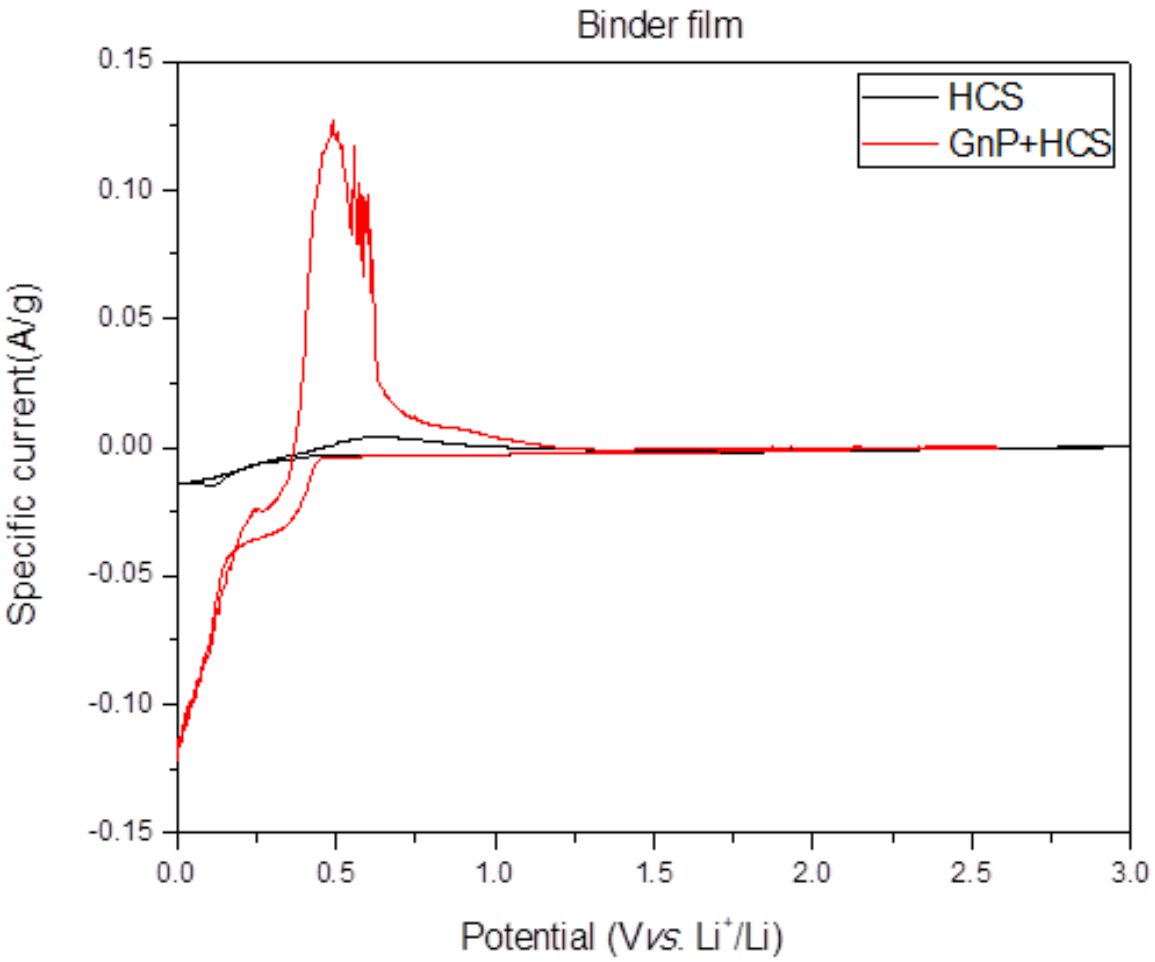

Figure 18. CV results of binder films.

3.2.2. LTO anode (LIBs)

3.2.2.1. Cycle and rate capability results

In the cycle test, all binders showed stable and almost similar capacities. In the rate capability test, the results including conductive material, super P, were as follows. At low current rate, all binders showed stable and similar capacities. However, at high current rate, HCS showed lower capacity than others. At all rates, GnP+HCS showed higher capacity than HCS. The results not including conductive material were as follows. At all rates, CS showed the highest capacity, and GnP+HCS showed much higher capacity than HCS. This trend was thought to be due to the effect of GnP on conductivity. However, although it was expected that the effect of GnP could be clearly seen since there were no conductive materials, CS had the highest capacity. The reason for these results was thought to be that GnP interfered with the movement of electrons.

3.2.2.2. EIS results

From the EIS results, resistance of bulk solution (R_s), charge transfer resistance (R_{ct}) and resistance to the bulk of active material which is also called Warburg impedance (R_{diff}) could be observed.

$$Z_{re} = R_s + R_{ct} + R_{diff}$$

First point of semicircle is R_s. And diameter of the semicircle is R_{ct}. Finally R_{diff} is the length of the 45° straight line in the end of graph before slope suddenly changes. Fresh cell at OCV and cells after charge/discharge of 0.1C and 0.5C were measured. First, in fresh cell at OCV, the charge transfer resistance of GnP+HCS and HCS was smaller than CS and 400B. However, after charge/discharge of 0.1C and 0.5C, CS showed the smallest charge transfer resistance. It was expected that electrons jump between electrolyte and electrode would be easy and thus charge transfer resistance would be low due to hollow structure. However, the results were not as expected after charge/discharge.

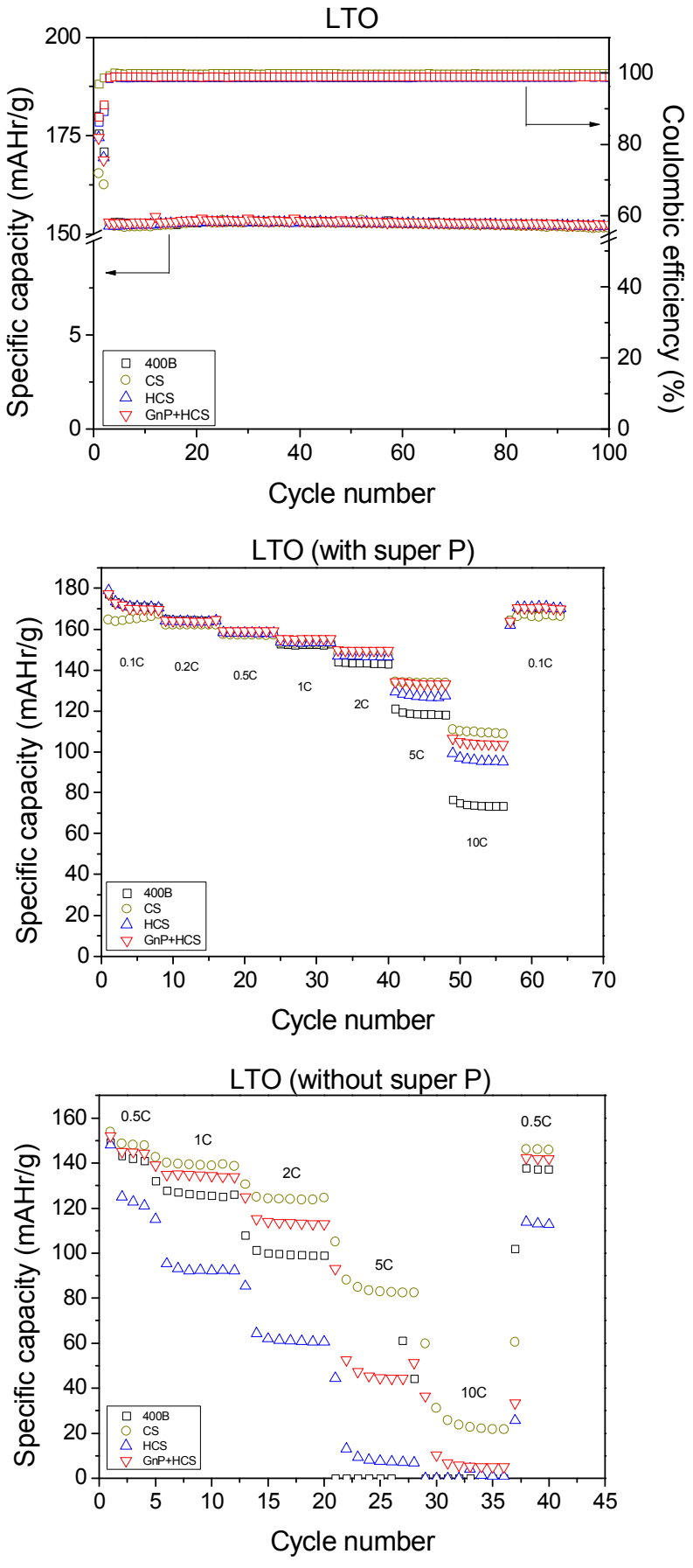

Figure 19. Cycle and rate capability results of LTO electrodes.

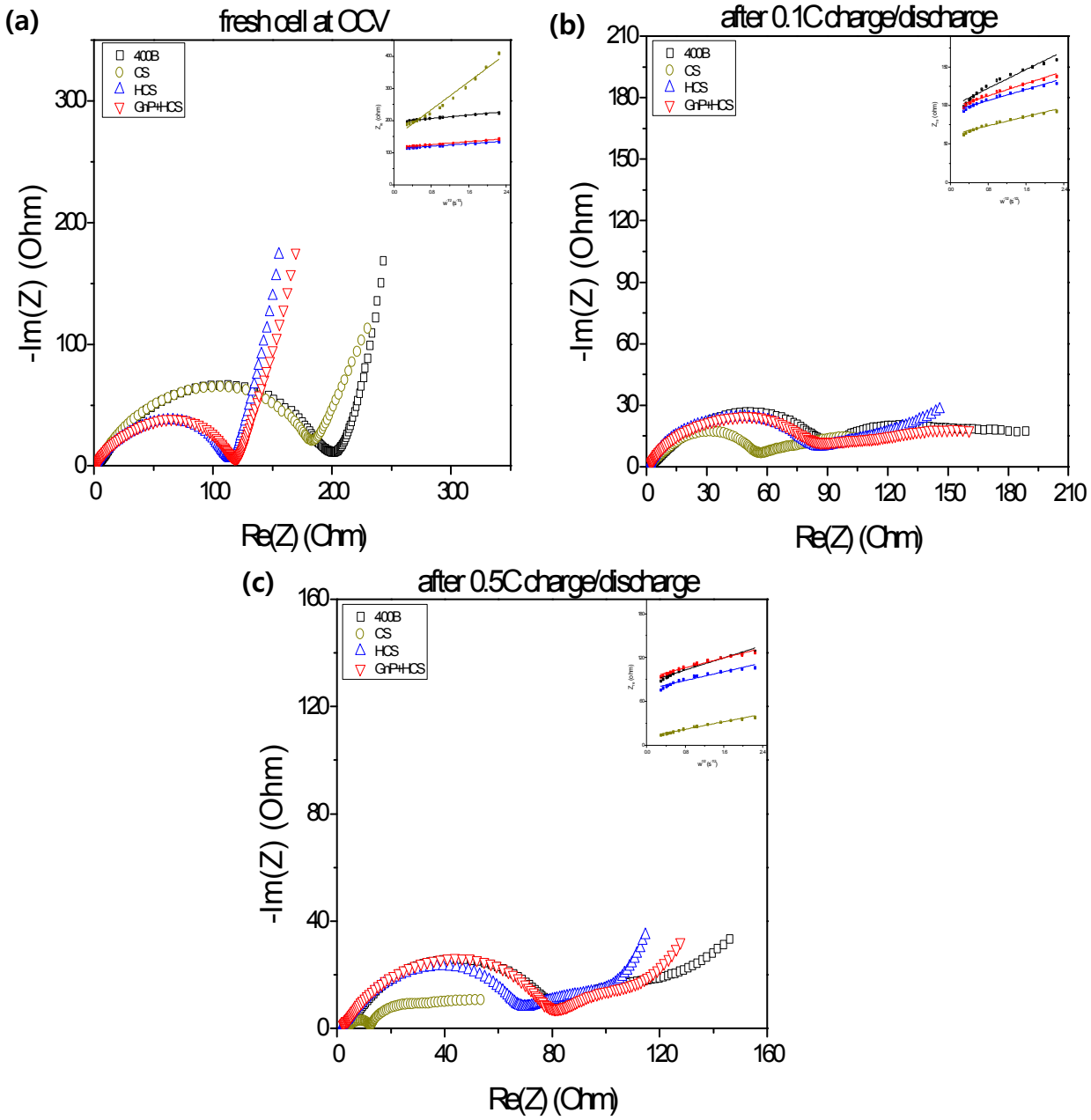

Figure 20. EIS results of LTO electrodes.

		Rs	Rct	1/Rct	D (x 10^{-11}) [cm^2/s]
fresh cell at OCV	400B	2.606	207	0.0048	8.5
	CS	1.97	186.2	0.0054	0.126
	HCS	1.039	116.6	0.0086	15.1
	GnP+HCS	1.24	120.4	0.0083	11
after 0.1C charge/discharge	400B	2.175	73.5	0.0163	1.6
	CS	1.397	62.7	0.0159	6.62
	HCS	1.185	76.26	0.0131	4.56
	GnP+HCS	1.025	96.12	0.0104	3.69
after 0.5C charge/discharge	400B	1,,628	68.47	0.0146	3.38
	CS	1.791	12.69	0.0788	8.8
	HCS	1.352	70.5	0.0142	6.49
	GnP+HCS	1.919	96.95	0.0103	5.07

Table 5. EIS results of LTO electrodes.

3.2.3. Si/C anode (LIBs)

3.2.3.1. Cycle and rate capability results

In the cycle test, CS showed the highest capacity and durability. As with the results of LTO, GnP+HCS showed higher capacity than HCS. The results of rate capability test were as follows. At low current rate up to 1C, CS showed the highest capacity, but at high current rate, CS was gradually unstable and then showed the lowest capacity. In addition, at high current rate, binder with hollow structure showed higher capacity than binder commercialized. It was thought that binder with hollow structure had somewhat controlled the volume change of silicon electrodes at high current rate and also GnP increased conductivity.

3.2.3.2. EIS results

EIS was also measured in the same situation as LTO. In every case, hollow binders showed lower resistance than CS. And also GnP+HCS showed lower resistance than HCS. As expected, it was thought that the electrons jump between electrolyte and electrode occurred more easily due to hollow structure. It might be also thought that GnP affected the movement of electrons.

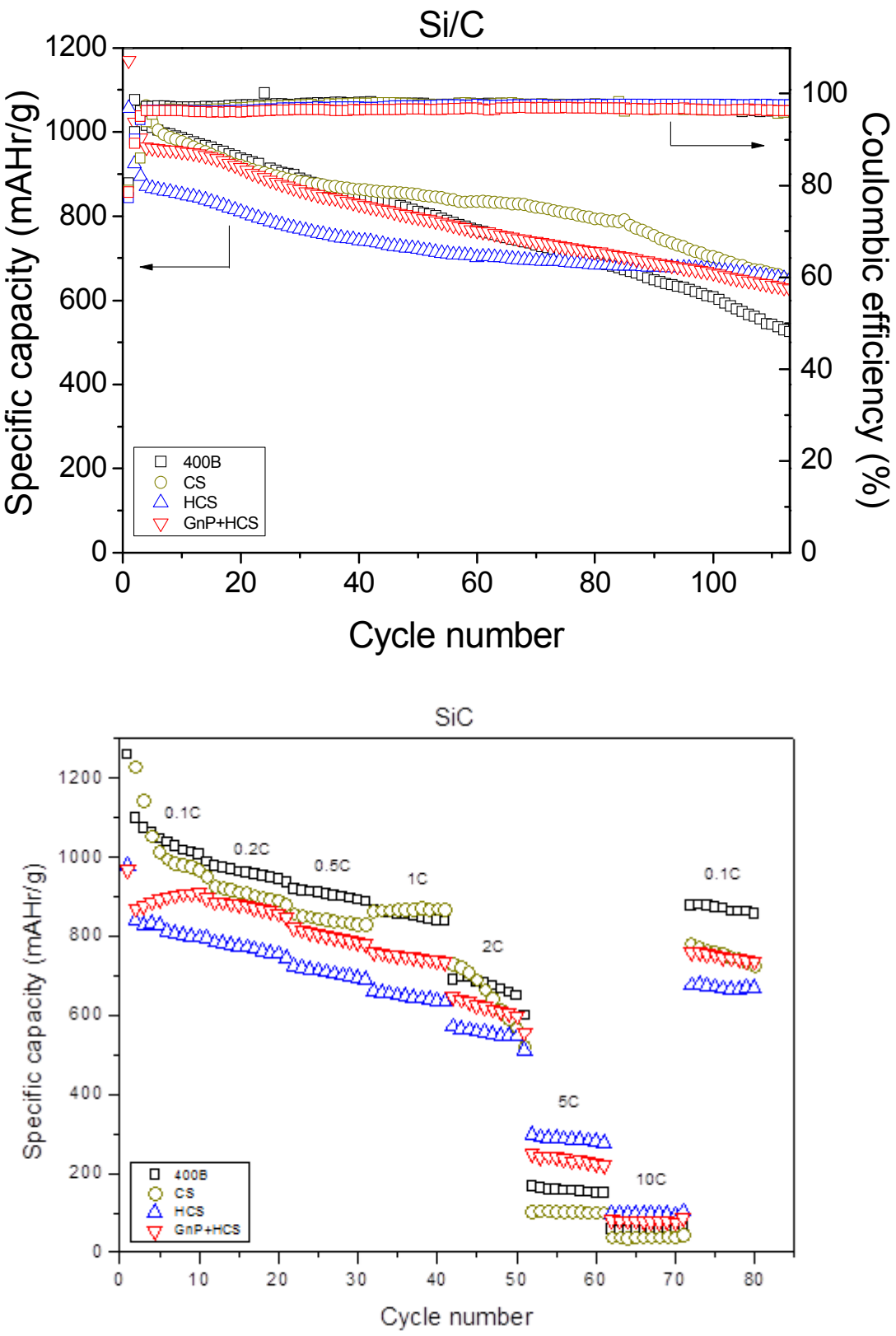

Figure 21. Cycle and rate capability results of Si/C electrodes.

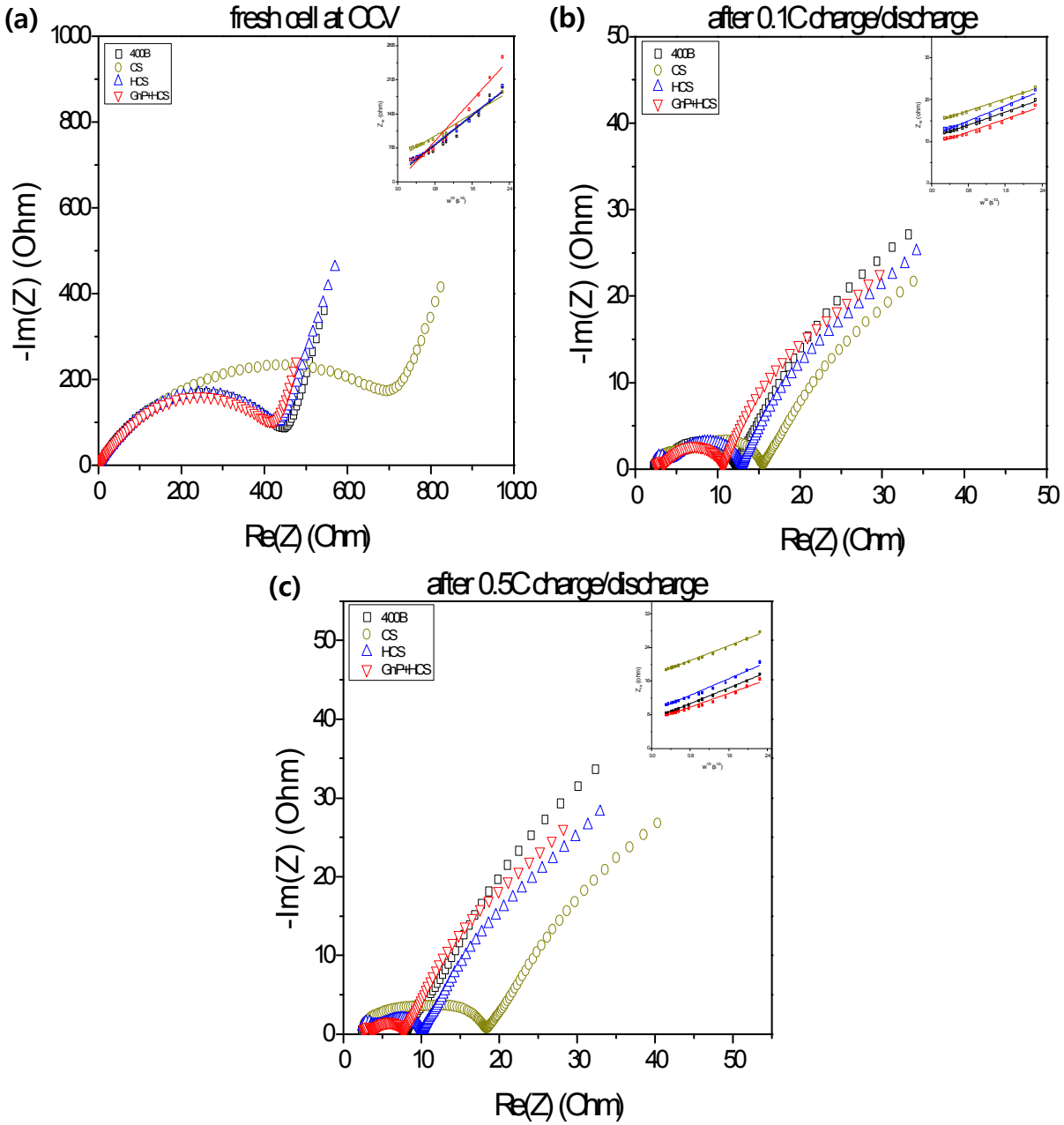

Figure 22. EIS results of Si/C electrodes.

		Rs	Rct	1/Rct	D (x 10^{-11}) [cm^2/s]
fresh cell at OCV	400B	2.048	48.5	0.0021	0.000195
	CS	1.788	764.4	0.0013	0.000343
	HCS	2.034	477.2	0.0021	0.000199
	GnP+HCS	2.939	446.1	0.0022	0.000101
after 0.1C charge/discharge	400B	2.275	10.13	0.0987	7.53
	CS	1.15	14.99	0.0667	8.6
	HCS	1.926	12.24	0.0817	5.48
	GnP+HCS	2.559	8.161	0.1225	7.65
after 0.5C charge/discharge	400B	2.341	6.262	0.1597	5.14
	CS	1.149	17.9	0.0559	5.8
	HCS	1.002	9.997	0.1000	4.64
	GnP+HCS	2.441	5.562	0.1798	6.78

Table 6. EIS results of Si/C electrodes.

3.2.4. Activated carbon electrode (EDLCs)

3.2.4.1. Cycle and rate capability results

In the cycle test, GnP+HCS showed the highest capacity. In the rate capability test, similar to the results of the cycle test, GnP+HCS showed the highest capacity and CS showed the lowest capacity. In other words, hollow binders showed higher capacities than CS. And GnP+HCS also showed higher capacity than HCS. When the hollow structured binder containing GnP was applied to electrodes of capacitor, the effect was the greatest.

3.2.4.2. EIS results

There was no redox reaction in EDLCs. Thus, there was no charge transfer resistance. Instead, the semicircle meant conductivity of ions from electrolyte to surface of activated carbon electrodes to create charge balance. EIS was measured for fresh cell and the cell charged with 1mAcm^{-2}. As shown in figure 24, the hollow binders showed smaller resistance than CS in both cases. This results were consistent with cycle and rate capability test.

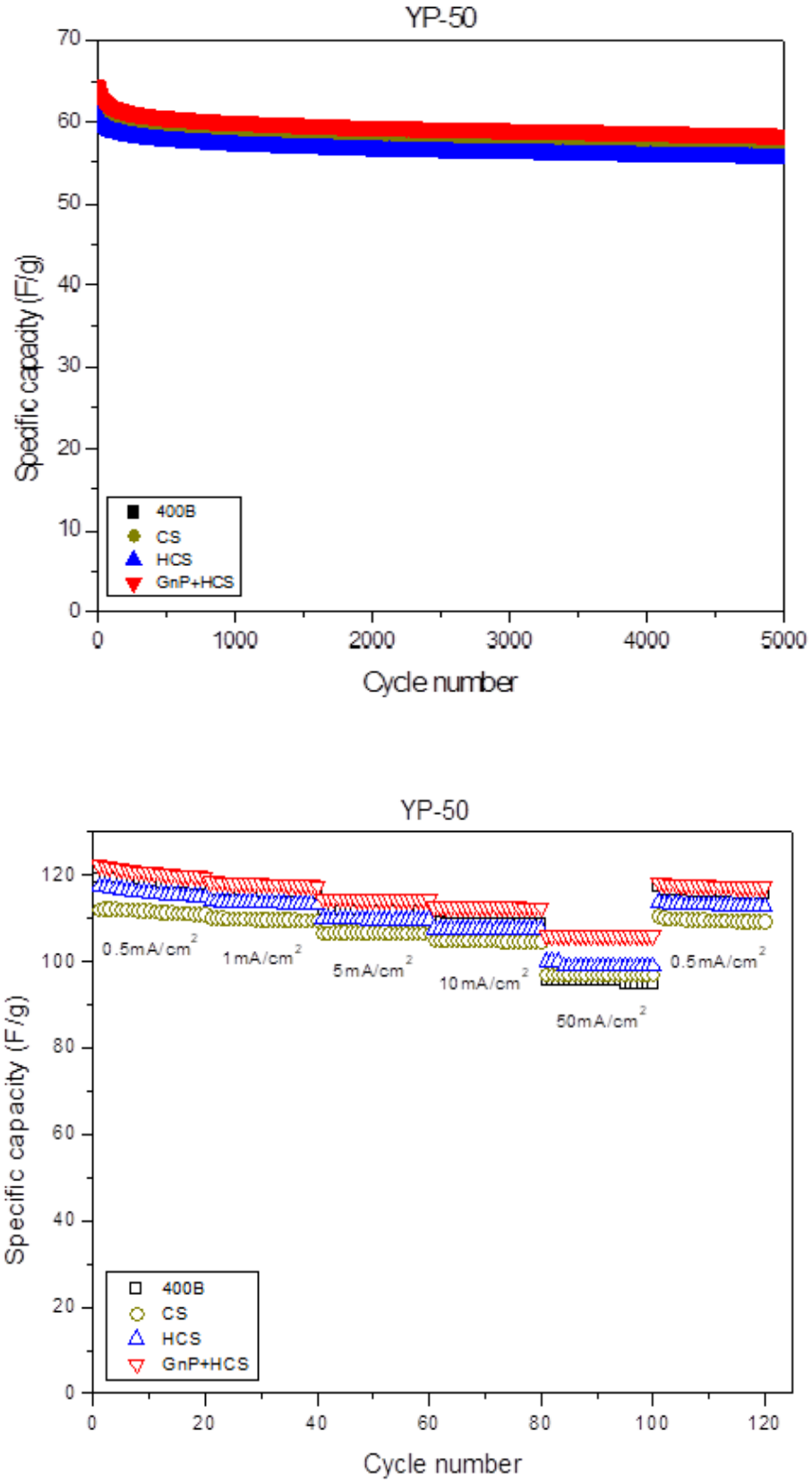

Figure 23. Cycle and rate capability results of activated carbon electrodes of EDLCs.

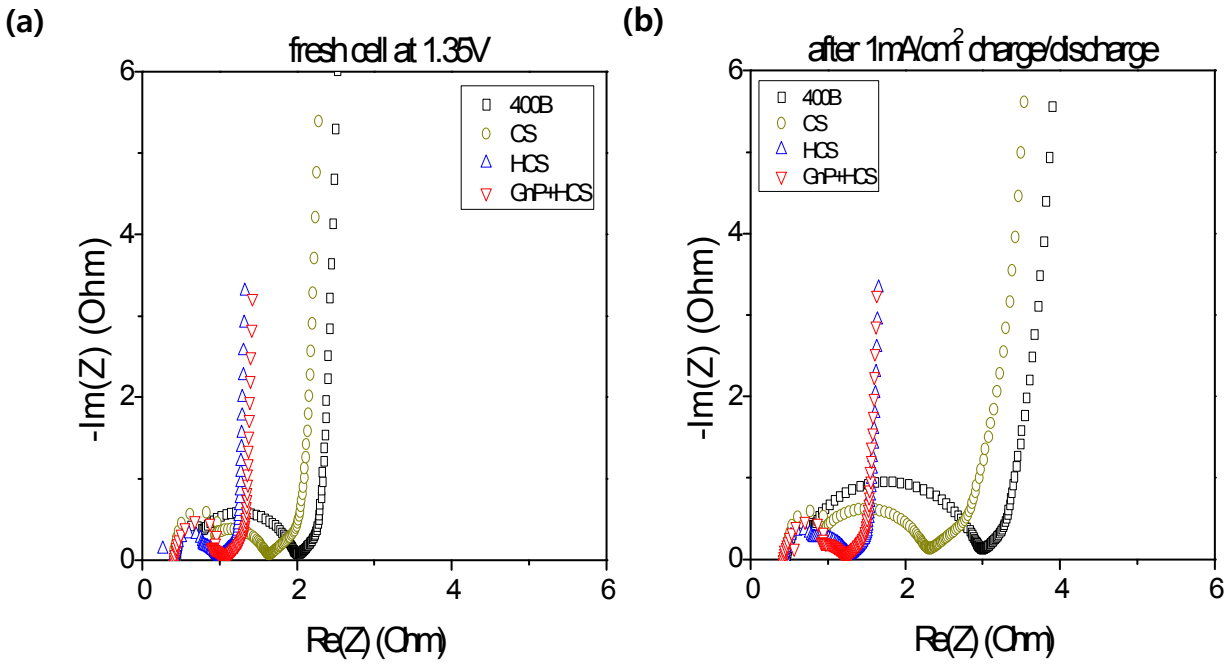

Figure 24. EIS results of activated carbon electrodes.

		Rct
fresh cell at 1.35V	400B	2.00
	CS	1.65
	HCS	1.01
	GnP+HCS	1.06
after $1mA/cm^2$ charge/discharge	400B	2.98
	CS	2.35
	HCS	1.30
	GnP+HCS	1.22

Table 7. EIS results of activated carbon electrodes.

4. Conclusion

After polymerizing the new conductive polymer complex binder with hollow structure, GnP+HCS, the binder was applied to LIBs and EDLCs electrodes. The CS, HCS without GnP, and GnP+HCS binders were compared and analyzed with commercial non-hollow SBR type binder.

Through physical analysis, the presence of GnP and hollow structure of binders were confirmed. And also the following have been identified : First, binders with hollow structure showed higher adhesion and electrolyte uptake than CS binder. Second, GnP+HCS showed higher electrical conductivity than HCS. Through electrochemical analysis, the following have been identified : First, when applied to Si/C and activated carbon electrodes except LTO electrodes, binders with hollow structure showed better performance than CS binder. Second, when applied to all electrodes, GnP+HCS normally had better performance than HCS.

5. Reference

[1] Zaghib, K., Mauger, A., Groult, H., Goodenough, J., Julien, C., 2013. Materials 6, 1028–1049.

[2] Nitta, N., Wu, F., Lee, J.T., Yushin, G., 2015. Materials Today 18, 252–264.

[3] Zhang, X., Zhang, H., Li, C., Wang, K., Sun, X., Ma, Y., 2014. RSC Adv. 4, 45862–45884.

[4] X Sun, X Zhang, H Zhang, B Huang, Y Ma, 2013. J. Solid State Electrochem. 17, 2035-2042.

[5] M. Zhi, C. Xiang, J. Li, M. Li, N. Wu, 2012. Nanoscale. 5, 72-88.

[6] L.L.Zhang, X.S.Zhao, 2009. Chem.Soc. Rev. 38, 2520-2531.

[7] Nordh, T., Younesi, R., Brandell, D., Edström, K., 2015. Journal of Power Sources 294, 173–179.

[8] R. Teranishi, Q. Si, F. Mizukoshi, M. Kawakubo, M. Matsui, Y. Takeda, O. Yamamoto and N. Imanishi, 2015. Journal of Power Source, 273, 538.

[9] J. Song, M. Zhou, R. Yi, T. Xu, M. Gordin, D. Tang, Z. Yu, M. Regula and D. Wang, 2014. Adv. Funct. Mater.,24, 5904.

[10] Shiraishi, S., 2013. 7.

[11] H. Zhao, Z. Wang, P. Lu, M. Jiang, F. Shi, X. Song, Z. Zheng, X. Zhou, Y. Fu and G. Abdelbast, 2014. Nano Letters, 14, 6704.

[12] Yuan, C.-D., Miao, A.-H., Cao, J.-W., Xu, Y.-S., Cao, T.-Y., 2005. Journal of Applied Polymer Science 98, 1505–1510.

[13] Zhang, Q., Yang, Z., Zhan, X., Chen, F., 2009. Journal of Applied Polymer Science 113, 207–215.

[14] Song, C., Zhang, L., Wang, Y., Yan, X., Zhao, D., 2013. Journal of Materials Science 48, 8153–8162.

[15] Y. Liu, Dr. K. V. Edmond, Dr. A. Curran, C. Bryant,Dr. B. Peng, Prof. D. G. A. L. Aarts, Dr. R. P. A. Dullens, Adv. Mater. 2016, 28, 8001–8006.

[16] Ramli, R.A., 2017. RSC Advances 7, 52632–52650.

[17] Lee, B.-R., Oh, E.-S., 2013.The Journal of Physical Chemistry C 117, 4404–4409.

[18] S. Lee and E.-S. Oh, 2013. Journal of Power Source, 244, 721.

[19] M. Ryou, J. Kim, I. Lee, S. Kim, Y. Jeong, S. Hong, J. Ryu, T. Kim, J. Park, H. Lee and J. Choi, 2013. Adv. Mater., 25, 1571.

[20] H.K. Park, B.S. Kong and E.-S. Oh, 2011. Electrochemistry Communications, 13, 1051.

[21] A. Magasinski, B. Zdyrko, I. Kovalenko, B. Hertzberg, R. Burtovyy, C.F. Huebner, T.F. Fuller, I. Luzinov and G. Yushin, 2010. ACS Appl. Mater. Interfaces, 2, 3004.

[22] S.L. Chou, J.Z. Wang, H.K. Liu, and S.X. Dou, 2011. J. Phys. Chem. C, 115, 16220.

[23] G.T. Kim, S.S. Jeong, M. Joost, E. Rocca, M. Winter, S. Passerini, and A. Balducci, 2011. J. Power Sources, 196, 2187.

[24] S. Lee, E.Y. Kim, H. Lee and E.-S. Oh, 2014. J. Power Sources, 269, 418.

[25] L. Gong, M.H.T. Nguyen and E.-S. Oh, 2013. Electrochemistry Communications, 29, 45.

[26] M.H.T. Nguyen and E.-S. Oh, 2013. Electrochemistry Communications, 35, 45.

[27] T. F. Yi, L. J. Jiang, J. Shu, C. B. Yue, R. S. Zhu, H. B. Qiao, 2010. J. Phys. Chem. Solids 71.

[28] M. Yoshio, R. J. Brodd, A. Kozawa, 2007. Lithium-ion batteries, Germany: Springer Verlag.